NUMERICAL SIMULATION OF STEEL DESULFURIZATION PROCESS IN THE GAS-STIRRED LADLE

by

Congshan Mao

A Thesis

Submitted to the Faculty of Purdue University

In Partial Fulfillment of the Requirements for the degree of

Master of Science in Mechanical Engineering

Department of Mechanical and Civil Engineering at Purdue Northwest

Hammond, Indiana

December 2021

THE PURDUE UNIVERSITY GRADUATE SCHOOL
STATEMENT OF COMMITTEE APPROVAL

Dr. Chenn Q. Zhou, Chair

Department of Mechanical and Civil Engineering at Purdue Northwest

Dr. Xiulin Wang

Department of Mechanical and Civil Engineering at Purdue Northwest

Dr. Ran Zhou

Department of Mechanical and Civil Engineering at Purdue Northwest

Approved by:

Dr. Chenn Q. Zhou

To the people I love

ACKNOWLEDGMENTS

I want to express my heartfelt gratitude to everyone who made it possible for me to complete my thesis. My advisor, Prof. Chenn Q. Zhou, deserves my utmost appreciation. Her superior professional abilities and expertise educated me, while her brilliant talents inspired me, and her severe demeanor impacted me. I can successfully complete the thesis with her diligent instruction and affirmation.

I'd like to convey my gratefulness to Prof. Xiulin Wang and Prof. Ran Zhou for their contributions to my thesis advising committee.

I would like to show my thankfulness to my colleagues in the Center for Innovation through Visualization and Simulation (CIVS) at Purdue University Northwest for their assistance and motivation. Dr. Armin Silaen and Mr. Nicholas Walla merit my special thanks for their invaluable and altruistic contributions to this project, and their professional advice has been extremely beneficial to me throughout my thesis study.

I would like to pay my respects to all members of the Steel Manufacturing Simulation and Visualization Consortium (SMSVC) for their assistance and cooperation throughout this study.

Finally, I want to express my thanks to my beloved parents for their unconditional support and considerate encouragement to my education.

TABLE OF CONTENTS

LIST OF TABLES

LIST OF FIGURES

LIST OF SYMBOLS

A	local area at the slag-steel interface (m^2)
$a_{Al_2O_3}$	alumina activity in slag
a_{Al}	aluminum activity in steel
a_O	oxygen activity in steel
C_D	drag coefficient
C_{e}	minimum bubble diameter (m)
C_S	sulfide capacity
c	constant
D	ladle diameter (m)
D_m	species diffusion coefficient in steel phase (m^2/s)
D_s	species diffusion coefficient in slag phase (m^2/s)
d	bubble diameter (m)
E_0	Eotvos number
$\mathrm{e}_{\mathrm{i}}^{\mathrm{j}}$	interaction parameter between element i and j
F_b	bubble force (N)
F_D	bubble drag force (N)
F_{VM}	bubble virtual mass force (N)
f_S	sulfur activity coefficient in steel phase
G_b	buoyancy turbulence kinetic energy (m^2/s^2)
G_k	velocity gradient turbulence kinetic energy (m^2/s^2)
g	gravitational acceleration (m/s^2)
J	molar flux ($mole/m^2s$)
k	turbulence kinetic energy (m^2/s^2)
$k_{\mathrm{e}ff}$	overall species mass transfer coefficient between steel phase and slag phase (m/s)
k_m	species mass transfer coefficient in steel phase (m/s)
k_s	species mass transfer coefficient in slag phase (m/s)
L_S	sulfur distribution ratio

M_{i}	molecular weight of species i (kg/mol)
n	oxygen atoms number in oxide
V	local steel phase volume at the slag-steel interface (m^3)
v	velocity (m/s)
Pr_t	turbulent Prandtl number
p	local pressure (Pa)
Q	volumetric flow rate (m^3/s)
Re	Reynolds number
r_1	collector bubble diameter in coalescence (m)
r_2	smaller bubble diameter in coalescence (m)
S	source term $(kg/m^3 s)$
Sc_t	turbulent Schmidt number
T	temperature (K)
t	time (s)
x	mole faction of oxide in slag
Y	local species mass fraction
$[wt-\%\mathrm{i}]$	mass fraction of element i in steel phase
$(wt-\%\mathrm{i})$	mass fraction of element i in slag phase
$[wt-\%\mathrm{i}]^*$	mass fraction of element i in steel phase at equilibrium state
$(wt-\%\mathrm{i})^*$	mass fraction of element i in slag phase at equilibrium state
α_m	volume fraction of continuous phase m
β	thermal expansion coefficient
ρ	density $(kg/m^3 s)$
σ	surface tension (N/m)
ε	turbulent dissipation rate (m^2/s^3)
Λ	optical basicity
μ	dynamic viscosity $(kg/m \cdot s)$
ν	kinematic viscosity (m^2/s)
ϑ	kinetic viscosity $(Pa \cdot s)$

τ_B	bubble breakup timescale (s)
τ_b	bubble relaxation timescale (s)
τ_C	bubble coalescence timescale (s)
τ_l	energetic turbulence eddies timescale (s)
τ_k	turbulence microscale (s)
τ_{rel}	additional turbulence microscale (s)

ABSTRACT

A three-dimensional isothermal multiphase flow transient CFD model simulation of the comprehensive chemical processes, including desulfurization and reoxidation in a gas-stirred ladle during the secondary refinement process, has been investigated. The multiphase interactions and turbulence flow among steel, slag, and gas inside a ladle are simulated based VOF multiphase model and discrete model (DPM) in Fluent commercial software. A widely used theory describing the desulfurization and reoxidation processes, (Al2O3) -[O] equilibrium theory, is introduced into the model. The compositions of both steel and slag are monitored, and the mass fractions of each species in steel and slag are compared with the industrial data. There are two main stages for this study.

In the first stage, the CFD model of an 80-ton ladle is developed to simulate both the flow field and reaction rates based on literature work. Then the predicated species contents are validated with industrial measurement, which proves the accuracy of the CFD model.

The validated CFD model is applied to a Nucor Decatur two plugs bottom injection ladle in the second stage. There are two different plug separation angle scenarios: 90° and 180°, investigated in this part. Three argon gas flow rate combinations ((5/5 SCFM, 5/20 SCFM, and 20/20 SCFM) were employed. The slag eye size was validated with plant measurement. The results show that the desulfurization rate and reoxidation rate are promoted with a higher argon injection rate. When the argon injection rate is fixed, a larger separation angle improves the reaction rates.

1. INTRODUCTION

Steelmaking is a crucial step in the production of high-quality steel before continuous casting. Primary steelmaking and secondary steelmaking are the two processes. The liquid iron is converted from a blast furnace and metal scrap during the primary steelmaking process and then transformed into low-carbon steel via a basic oxygen furnace or an electric arc furnace. The secondary steelmaking stage is a post-steelmaking process that refines steel with low carbon content at a separate station before casting. The ladle furnace (LF) is an important component of secondary steel production. The molten steel from primary steelmaking is received by the ladle, which subsequently undergoes inclusion removal and chemical adjustments, including the desulfurization.

Desulfurization has a significant impact on the quality of molten steel and, as a result, on the products. Surface fractures and weakness can be caused by high sulfur concentration, which reduces resistance and durability. Desulfurization agents such as calcium carbide, lime, and magnesium vapor or powder are used to remove sulfur effectively. However, due to resulfurization during the converter process, sulfur content will inevitably rise in the stages preceding secondary steelmaking. Desulfurization in secondary steelmaking is thus the final opportunity to adjust sulfur concentration in steel prior to continuous casting.

Desulfurization happens at the slag-steel interface in the secondary steelmaking process, where sulfur in the steel reacts with lime particles in the slag. Desulfurization rate is influenced by a variety of factors, including steel velocity and turbulence, slag physical characteristics, local sulfur content distribution, and species transfer, according to many studies. As a result, it's critical to comprehend steel-slag reactions and the pace of desulfurization under various thermodynamic and hydrodynamic settings.

1.1 Literature Review

Many research pieces have been carried out in ladle metallurgy desulfurization, including experimental work and numerical simulation to investigate the effect of related parameters on chemical reactions during the secondary steelmaking process. El-Kaddah and Szekely [1] proposed a basic desulfurization prediction model between slag and steel, where the slag-

steel interface was assumed to be a flat free surface. In 1985, BAN-YA [2] proposed a regular solution method to predicate the values of oxide activity based on the interaction energy between cations in slag, which affects the sulfur mass fraction between slag and steel at the equilibrium state, and the theory was proved to be validated compared to experimental works. The reaction equilibrium constant of the dissolved element in steel was also developed, which indicates the reaction rate at equilibrium status. These works revealed the influence of slag compositions on physical characters and steel temperature on the chemical potential, which lays a deep foundation for further investigations of chemical processes in a ladle. In 1993, BAN-YA [3] improved the regular solution model by adding a conversion factor of activity coefficient so that the model was satisfied over a wide range of slag composition from basic to acidic sides. In the territory of the desulfurization study, the sulfide capacity, which describes the desulfurization kinetics ability of metallurgical slag proposed by Richardson and Fincham [4], was further investigated by Sosinsky and Sommerville [5]. They proposed a method to estimate sulfide capacity based on slag compositions and the optical basicities, which is named as the S-S model. Later the S-S model was improved by Young [6], and a more comprehensive model has been proposed to predicate the sulfide capacity. Andersson [7] summarized different ways of sulfide capacity estimation, including the S-S model and KTH model, and discussed their reliability compared with plant trials. In order to have more comprehensive investigations about the reactions between slag and steel, JONSSON [8] built a CFD model to simulate the chemical reactions during the gas-stirring process, where the oxygen activity used for reaction rate calculation was assumed to be controlled by the [Al]-[O]-(Al_2O_3) equilibrium at the slag-steel interface. It was found that the reaction rate was determined by the species transfer rate between slag and steel. However, this study only focused on the concentration change of S and Al in steel, and the slag impact was ignored, where a flat surface was constructed to represent the slag-steel interface. ANDERSSON [9] proposed a 2D CFD model, where the slag was considered, and the activities of oxides in slag were investigated. Then the effect of compositions on slag and temperature on steel were studied [10]. Pär G. JÖNSSON and Lage T. I. JONSSON [11] summarised the desulfurization, reoxidation, and inclusion removal models. They claimed that even though there was not an overall model to predict desired parameters of all the

steps in the steel refining process, the existing models could be helpful to predicate each parameter respectively. In 2002, Andersson [12] proposed a static numerical model, which showed good agreement with both CFD simulation results and plant data. Though static modeling does not reflect local species concentration as the CFD model simulates, it costs less time than a typical CFD simulation. Conejo [13] modified the static mathematical model by updating the oxygen activity expression based on the equilibrium of multiple reactions at the slag-steel interface, including (Al_2O_3)-(FeO)-(SiO_2)-(MnO)-[O]-[S]. This method is more comprehensive and accurate in predicting oxygen activity, but it necessitates a specific iteration calculation procedure, demanding more computational power and time. Lou [14] built a 3D computational fluid dynamics-simultaneous reaction model (CFD-SRM) coupled model to predicate the desulfurization and alloying element reactions during the gas stirring process in a ladle. In this model, the slag-steel interface is a flat surface, and the slag layer is not built in the computational domain; instead, the influence of slag on desulfurization is introduced to the model by user-defined functions. The oxygen activity is also determined by (Al_2O_3)-(FeO)-(SiO_2)-(MnO)-[O]-[S] equilibrium. The effects of oxygen absorption at the slag eye area on oxygen activity are taken into account. The results show a high level of agreement with measured data. Cao [15] established a quick estimation model to evaluate the desulfurization kinetics in a gas-stirred ladle, including a transient CFD model and a static mathematical model. The flow field, slag eyes, and slag-steel interaction features are obtained through CFD simulation, and then the chemical reaction rates are computed by the static multicomponent reaction kinetics model. This model is suitable for rapid inspection, but the simulation accuracy is not as excellent as the coupled model because the local sulfur content distribution is disregarded. Then a more comprehensive CFD model is proposed by Cao [16]. The flow field is generated using the VOF-DPM multiphase model, and the slag eye size and slag-steel interface shape vary over time, with the desulfurization rate updated in each step coupled with the flow, accurately representing the practical desulfurization procedure in a gas-stirred ladle. However, because both the flow field and reaction information are solved by transient models, this model necessitates a lot of computational resources.

1.2 Objective

Based on the previous studies, it is acceptable to conclude that existing CFD models can accurately predict the desulfurization process in a gas-stirred ladle. In most cases, however, the slag-steel interface is considered a flat surface, and the slag eye size is computed based on empirical expressions, which is limited by the scope of the formula application, and it is hard to determine the slag eye locations in the computational domain. The transient VOF-DPM model can predict the surface shape and slag eye size over time, but it demands high computing effort to update the flow field in each step. In order to meet the industrial application requirements, a method is needed to obtain the slag eye size and the interface shape during the treatment with fewer computational requirements and less time. In this work, a quasi-steady-state flow field is employed to model the slag eye size and position and the interface shape in a ladle.

Desulfurization is one of the primary goals of chemical adjustment during secondary steelmaking, and oxygen activity is a crucial parameter for estimating the sulfur reaction rate. The (Al_2O_3)-(FeO)-(SiO_2)-(MnO)-[O]-[S] equilibrium approach provides more complete oxygen activity results, but it takes longer to compute due to the iteration process. It is found that the [Al]-[O]-(Al_2O_3) equilibrium approach produces comparable results to those obtained by (Al_2O_3)-(FeO)-(SiO_2)-(MnO)-[O]-[S] equilibrium method in terms of desulfurization prediction, but with easier calculation procedures. Therefore, the current model is subjected to the (Al2O3)-[Al]-[O] equilibrium approach.

The goal of this paper is to develop a three-dimensional CFD model for predicting the flow field and desulfurization process in a gas-stirred ladle. The flow field information based on a Nucor generic ladle at the quasi-steady state will be obtained under various stirring scenarios. After being validated by industrial measurement, the flow field will combine the species transport model to yield the local sulfur content distribution. Then the desulfurization rates will be calculated at the slag-steel interface to determine the sulfur removal rate during treatment, and the source terms will be introduced to the species transport model. The effects of various stirring scenarios on the desulfurization rate are expected to be investigated, and recommendations for optimizing the operation parameters are supposed to be made.

Finally, the effect of temperature and initial slag composition on desulfurization rate is under discussion to optimize sulfur content management.

2. METHODOLOGY AND CFD MODEL

In this study, the flow field of the steel/slag/argon multiphase flow is solved and the sulfur content is obtained, and then the sulfur removal rate is determined and applied to the CFD model to complete the desulfurization simulation process.

2.1 Multiphase Flow

In this study, the VOF (Volume of Fluid) model in Euler-Euler approach is used to simulate the multiphase flow of two continuous phases: steel and slag. The argon is considered to be a discrete phase and the DPM (Discrete Phase Model) model is introduced into the simulation to calculate the interactions between continuous phases and discrete phase. The Species Transport model is used to calculate the species content distribution in the continuous phase.

2.1.1 VOF Model

In Euler-Euler approach, the VOF method can model multiphase flows that are immiscible by solving one single momentum equations. It tracks the volume fraction of each phase in the domain and obtains the surfaces between phases and determines the interface positions. The continuity equation for phase m is written in the following expression:

$$\frac{1}{\rho_m}\left[\frac{\partial}{\partial t}\left(\alpha_m \rho_m\right) + \bigtriangledown \cdot \left(\alpha_m \rho_m \vec{v}_m\right)\right] = 0 \tag{2.1}$$

where α_m is the volume fraction of phase m. The volume fraction equation for the primary phase is not solved; instead, the primary phase volume fraction can be obtained based on the principle that the volume fractions of all phases sum to unity shown in the following expression:

$$\sum_{m=1}^{\mathrm{i}} \alpha_m = 1 \tag{2.2}$$

For the momentum conservation, the following equation is solved in VOF model:

$$\frac{\partial}{\partial t}\left(\rho\vec{v} + \bigtriangledown \cdot \rho\vec{v}\vec{v}\right) = -\bigtriangledown p + \bigtriangledown \cdot \left[\mu\left(\bigtriangledown\vec{v} + \vec{v}^{T}\right)\right] + \rho\vec{g} + \vec{F}_b \tag{2.3}$$

where μ is the mixture viscosity of continuous phases; $\vec{v}$ is the velocity of liquid flows; p is the the local pressure; $\vec{g}$ is the local gravity acceleration; F_b is the bubble force exerted on the mixture continuous fluids.

2.1.2 Discrete Phase Model

The argon is considered to be a discrete phase in this study, and the Discrete Phase Model (DPM) is used to calculate the trajectory of each bubble in each time step by solving the force balance including drag force, buoyancy force, virtual mass force and pressure gradient force based on Euler-Lagrange approach shown as follows:

$$\frac{d\vec{v}_p}{dt} = F_D\left(\vec{v} - \vec{v}_p\right) + \frac{\vec{g}\left(\rho_p - \rho\right)}{\rho_p} + \vec{F}_{VM} + \vec{F}_{pressure} \tag{2.4}$$

where $\vec{v}$ is the continuous phase velocity and $\vec{v}_p$ is the discrete particle velocity, respectively.

The first term on the right hand in Equation 2.4, $F_D\left(\vec{v} - \vec{v}_p\right)$, indicates the drag force per unit particle mass. F_D is obtained by the following expression:

$$F_D = \frac{18\mu}{\rho_m d_p^2}\frac{C_D Re}{24} \tag{2.5}$$

where d_p is the particle diameter; μ is the fluid viscosity;. Re is the particle Reynolds number based on the particle diameter and relative fluid velocity and can be written in the following format:

$$Re = \frac{\rho d_p |v - v_p|}{\mu_l} \tag{2.6}$$

C_D is the drag coefficient and can be written in the following expression based on Hamathy's theory [17]:

$$C_D = \frac{2}{3}\left(\frac{E_0}{3}\right)^{0.5} \tag{2.7}$$

where E_0 is Eotvos number describing the relationship between buoyancy force and particle surface tension and can be calculated by the following equation:

$$E_0 = \frac{g\left(\rho - \rho_p\right) d_p^2}{\sigma} \tag{2.8}$$

where σ is the surface tension between continuous phases and discrete phase.

The virtual mass force, $\vec{F}_{VM}$, describes the acceleration of fluids surrounding the particle and is expressed as:

$$\vec{F}_{VM} = \frac{1}{2}\frac{\rho}{\rho_p}\left(\vec{v}_p \bigtriangledown \vec{v} - \frac{d\vec{u}_p}{dt}\right) \tag{2.9}$$

If the mixture density of continuous phases is bigger than that of the discrete phase, an additional force that comes from the pressure gradient will be applied to the continuous fluids and can be expressed as:

$$F_{pressure} = \left(\frac{\rho}{\rho_p}\right)\vec{v}_p \bigtriangledown \vec{v} \tag{2.10}$$

where $\vec{v}$ is the fluid velocity; $\vec{v}_p$ is the particle velocity; ρ and ρ_p are the density of continuous phase and discrete phase, respectively.

In order to build a more comprehensive multiphase interaction model, the random walk model in the DPM method is employed to represent the turbulent dispersion of the particle exerting on the liquid velocity. The two-way turbulence coupling is also applied to the particle accounting for the momentum exchange between continuous phases and discrete phase.

Besides momentum transfer between phases, the collision, coalescence, and breakup impacts between two particles are taken into consideration. During the rising process, two bubble particles collide with each other and coalesce into one bubble with a bigger diameter. Affected by several factors, the bubble will breakup into smaller particles when it reaches the equilibrium diameter under the current circumstance.

The bubble particle is treated as sphere and the maximum bubble diameter at the plug is determined by the argon flow rate [18] as shown in the following equation:

$$d_{b,max} = 0.35 \left(\frac{Q^2}{g} \right)^{0.2} \tag{2.11}$$

where Q is the gas volumetric flow rate. The average bubble diameter is assumed to be 25 % of the maximum diameter [19], which is the initial diameter of the discrete phase in this study.

The probability of coalescence is determined by the critical Weber number and the radium of the collector $r1$ and of the smaller bubble $r2$ as shown below:

$$b_{crit} = (r_1 + r_2) \sqrt{min \left(1.0, \frac{2.4f}{We_{crit}}\right)} \tag{2.12}$$

where f is calculated by the following equation:

$$f = \left(\frac{r_1}{r_2} \right)^3 - 2.4 \left(\frac{r_1}{r_2} \right)^2 + 2.7 \left(\frac{r_1}{r_2} \right) \tag{2.13}$$

In the bubble breakup model, when the bubble diameter is over an equilibrium diameter, it will breakup into smaller particles with a new diameter. The equilibrium diameter can be calculated based on bubble surface tension and turbulence dissipation rate as shown below:

$$d_b^{eq} = 4\alpha_b^{0.5} \frac{\left(\frac{\sigma}{\rho}\right)^{0.6}}{\varepsilon^{0.4}} + C_{\mathrm{e}} \tag{2.14}$$

where α_b is the volume fraction of bubble; C_{e} stands for the minimum bubble diameter proposed by Pan [20] and it is 0.0001 m in this study. The bubble size variation is also under the influence of the relaxation time. The relaxation time indicates the time for the bubble growth or from the current diameter to the equilibrium diameter. Once the diameter is bigger than the equilibrium size, the breakup happens and several smaller bubbles are formed. The relaxation time can be determined by the following expressions:

$$\tau_{rel} = \begin{cases} \tau_B, d_b > d_b^{\mathrm{e}} \\ \tau_C, d_b < d_b^{\mathrm{e}} \end{cases} \tag{2.15}$$

where τ_B and τ_C represents the breakup timescale and coalescence timescale, respectively, and they can be obtained by the following equations:

$$\tau_B = d_b^{\frac{2}{3}} \varepsilon^{-\frac{1}{3}} \tag{2.16}$$

$$\tau_C = 2\left[\frac{\pi\left(\alpha_{b,max} - \alpha_b\right)}{6\alpha_b}\right]^{\frac{1}{3}} \frac{d_b}{\sqrt{\frac{2}{3}k}} \sqrt{1 + \frac{\tau_b}{\tau_l}} \tag{2.17}$$

$$\tau_b = \sqrt{\frac{\vartheta_l}{\varepsilon}} \tag{2.18}$$

$$\tau_l = \frac{\rho_b d_b^2}{18\mu_l} \tag{2.19}$$

where k is the turbulence kinetic energy; τ_b and τ_l are the bubble relaxation timescale and energetic turbulence eddies timescale, respectively; ϑ_l stands for the fluids kinetic viscosity; μ_l is the dynamic viscosity of the continuous phases. In addition, the turbulence microscale is introduced to Equation 2.15 to modify the relaxation time [19], which can be written as:

$$\tau_{rel} = max\left(\tau_{rel}, \tau_K\right) \tag{2.20}$$

where τ_K represents the turbulence microscale and can be obtained through the following expression:

$$\tau_K = 6\sqrt{\frac{\vartheta_l}{\varepsilon}} \tag{2.21}$$

2.1.3 Turbulence Model

In this study, the realizable $k - \varepsilon$ model is used to account for the turbulence flow in both Euler-Euler approach and Euler-Lagrange approach. The conservation equations of turbulence kinetic energy and turbulence dissipation rate are shown below:

$$\frac{\partial}{\partial t}\left(\rho k\right) + \frac{\partial}{\partial x_m}\left(\rho k u_m\right) = \frac{\partial}{\partial x_n}\left[\left(\mu + \frac{\mu_t}{\sigma_k}\right)\frac{\partial k}{\partial x_n}\right] + G_k + G_b - \rho\varepsilon + S_k \tag{2.22}$$

$$\frac{\partial}{\partial t}(\rho\varepsilon) + \frac{\partial}{\partial x_m}(\rho\varepsilon u_m) = \frac{\partial}{\partial x_n}\left[\left(\mu + \frac{\mu_t}{\sigma_\varepsilon}\right)\frac{\partial \varepsilon}{\partial x_n}\right] - \rho C_1 S_\varepsilon - \rho C_2 \frac{\varepsilon^2}{k + \sqrt{\nu\varepsilon}} + C_1 \frac{\varepsilon}{k} C_{3\varepsilon} C_b + S_\varepsilon \tag{2.23}$$

$$C_1 = max\left[\frac{\Phi}{5+\Phi}, 0.43\right] \tag{2.24}$$

$$\Phi = S\frac{k}{\varepsilon} \tag{2.25}$$

$$S = \sqrt{2S_{mn}S_{mn}} \tag{2.26}$$

$$S_{mn} = \frac{1}{2}\left(\frac{\partial u_n}{\partial x_m} + \frac{\partial u_m}{\partial x_n}\right) \tag{2.27}$$

where G_k and G_b are the turbulence kinetic energy that come from velocity gradient and buoyancy, respectively. $C_{1\varepsilon}$ and C_2 are constants in this model. S_k and S_ε are the source terms of turbulence kinetic energy and turbulence dissipation rate, respectively. S is the mean rate of strain tensor that can leads to the C_1.

$$G_k = -\rho\overline{u_t' u_l'}\frac{\partial u_n}{\partial x_m} \tag{2.28}$$

$$G_b = \beta g_m \frac{\mu_t}{Pr_t}\frac{\partial T}{\partial x_m} \tag{2.29}$$

where Pr_t is the turbulent Prandtl number for energy and it is 0.85 in the realizable $k-\varepsilon$ model; g_m is the component of the gravitational vector in the direction; β represents the coefficient of thermal expansion and can be calculated by the following equation:

$$\beta = -\frac{1}{\rho}\left(\frac{\partial \rho}{\partial T}\right)_P \tag{2.30}$$

μ_t stands for the eddy viscosity and can be calculated by the following equation:

$$\mu_t = \rho C_\mu \frac{k^2}{\varepsilon} \tag{2.31}$$

where C_μ in realizable $k-\varepsilon$ model is obtained from:

$$C_\mu = \frac{1}{A_0 + A_S \frac{kU}{\varepsilon}} \tag{2.32}$$

where A_0 is 4.04 in this study, and $A_S = \sqrt{6}\cos\Phi$.

$$U = \sqrt{S_{mn}S_{mn} + \tilde{\Omega}_{mn}\tilde{\Omega}_{mn}} \tag{2.33}$$

In Equation 2.23, the term $C_{3\varepsilon}$ accounts for the proportion of the buoyancy's impacts on ε, and can be computed by the following equation:

$$C_{3\varepsilon} = \tan h|\frac{\nu}{v}| \tag{2.34}$$

where ν is the flow viscosity and v is the flow velocity along the gravitational vector. The other constants in Equation 2.23 are $C_{1\varepsilon} = 1.44$, $C_2 = 1.9$, $\sigma_k = 1.0$, and $\sigma_\varepsilon = 1.2$.

2.1.4 Species Transport Model

To predicate the species local mass fraction and the transfer rate in the same phase or between continuous phases, the species transport model is used in this study. In the Eulerian-Eulerian multiphase flow, the conservation equation for species transport model takes the following form:

$$\frac{\partial}{\partial t}(\rho Y_{\mathrm{i}}) + \bigtriangledown(\rho \vec{v} Y_{\mathrm{i}}) = \bigtriangledown \cdot \left(\frac{\mu_t}{Sc_t}(\bigtriangledown Y_{\mathrm{i}})\right) + S_{\mathrm{i}} \tag{2.35}$$

where ρ, ν_t and $\vec{v}_t$ are the fluid mixture density, turbulent viscosity and velocity of continuous phases, respectively; Y_{i} is the local mass fraction of each species in the continuous liquids;S_{i}

is the source term of species i due to the species exchange at the slag-steel interface; Sc_t is the turbulent Schmidt number and it is 0.7 by default.

2.2 Desulfurization Rate Determination

At the slag-steel interface, the dissolved sulfur in steel reacts with lime in slag [21], and the desulfurization expression can be written as follows:

$$[S] + (CaO) = [O] + (CaS) \tag{2.36}$$

where [] stands for the species from the steel and () represents the species in slag [21]. The desulfurization rate is mainly affected by two aspects: (1) the difference of sulfur mass fraction between the current stage and the equilibrium stage; (2) the sulfur transport and supplement rates from the steel to the slag-steel interface. In order to obtain the desulfurization rate, it is necessary to know the potential concentration difference between the current state and equilibrium state, which is defined by the element distribution ratio.

2.2.1 Element Distribution Ratio

At the slag-steel interface, the ratio of element i mass fraction in steel and element i mass fraction in slag at equilibrium is written as:

$$(\% - \mathrm{i})^* = L_{\mathrm{i}} \, [\% - \mathrm{i}]^* \tag{2.37}$$

where $(\% - \mathrm{i})$ is the local mass fraction of element i from slag and $[\% - \mathrm{i}]$ is the local mass fraction of element i in steel; L_{i} indicates the distribution ratio between $(\% - \mathrm{i})$ and $[\% - \mathrm{i}]$. The asterisk $*$ means the value is at the equilibrium status.

The theoretical value of L_S can be calculated as follows [10]:

$$\log L_S = \log \frac{(\% - S)^*}{[\% - S]^*} = -\frac{935}{T} + 1.375 + \log C_S + \log f_S - \log a_O \tag{2.38}$$

where T is the temperature at the slag-steel interface. C_S stands for the sulfide capacity. a_O and f_S are the oxygen activity and the activity coefficient of sulfur in steel, respectively.

There are several models to predicate C_S, including trail measurement[8] and mathematical model[6], [10]. In this study, C_S is determined by Young's model[6] as shown below:
if $\Lambda < 0.8$

$$\log C_S = -13.913 + 42.84\Lambda - 23.82\Lambda^2 - \frac{11710}{T} - 0.02223\,(\% - SiO_2) \tag{2.39}$$

if $\Lambda \geq 0.8$

$$C_S = -0.6261 + 0.4804\Lambda + 0.7197\Lambda^2 + \frac{1697}{T} - \frac{2587\Lambda}{T} + 0.0005144\,(\% - FeO) \tag{2.40}$$

where Λ is the optical basicity and defined as follows [22]:

$$\Lambda = \frac{\sum x_1 n_1 \Lambda_1 + x_2 n_2 \Lambda_2 + \ldots}{\sum x_1 n_1 + x_2 n_2 + \ldots} \tag{2.41}$$

where Λ_{th} is the optical basicity of individual oxide in slag [23], [24] including CaO, Al_2O_3, MnO, MgO, SiO_2, FeO, and the value is summarized in Table 2.1; x_{th} indicates the mole fraction of individual oxide and n_{th} is the number of oxygen atoms associated with acidic and basic oxides, respectively.

Table 2.1. Optical basicity of individual oxides

	Al_2O_3	CaO	FeO	MgO	MnO	SiO_2
Λ_{th}	0.61	1.0	0.51	0.78	0.59	0.48

The activity coefficient f_{i} in steel can be obtained by the following expression[13]:

$$\log f_{\mathrm{i}} = \sum_{\mathrm{j}} \mathrm{e}_{\mathrm{i}}^{\mathrm{j}}\,[\% - \mathrm{i}] \tag{2.42}$$

where i and j represent the dissolved element S, Al, Mn, Si, C and O in steel. $\mathrm{e}_{\mathrm{i}}^{\mathrm{j}}$ stands for the interaction parameters between element i and j [25], which are listed in Table 2.2.

Table 2.2. Interaction parameters

	C	Si	Al	Mn	O	S
C	0.124	0.08	0.043	-0.012	-0.34	0.046
Si	0.18	0.11	0.058	0	-0.23	0.056
Al	0.091	0.0056	0.045	0	-6.6	0.03
Mn	-0.07	0	0	0	-0.083	-0.048
O	-0.45	0.131	-3.9	-0.021	0	-0.131
S	0.11	0.063	0.035	-0.026	-0.27	-0.028

The element activity a_{i} in steel can be written as follows:

$$a_{\mathrm{i}} = f_{\mathrm{i}}\,[\% - \mathrm{i}] \tag{2.43}$$

where i stands for the dissolved element Al, Mn, Si, C in steel. a_{Fe} is assumed to be the mole fraction of iron in steel [26]. There are several methods to estimate the oxygen activity a_O during the desulfurization process[14] [26] [27]. In this study, it is assumed that the oxygen activity is controlled by the [Al]-[O]-(Al_2O_3) equilibrium at the slag-steel interface [27], and can be calculated by the following equation:

$$\log a_O = \frac{1}{3}\log a_{Al_2O_3} - \frac{2}{3}\log f_{Al} - \frac{2}{3}\log\left[\% - Al\right] - \frac{15100}{T} + 3.87 \tag{2.44}$$

where $a_{Al_2O_3}$ is the alumina activity in slag, and can be obtained by a fitting function [27]:

$$a_{Al_2O_3} = 0.3 - 3.99342\mathrm{e}^{-0.0018T} \tag{2.45}$$

2.2.2 Mass Transfer Coefficient

In secondary steelmaking, the desulfurization rate at the slag-steel interface is affected by thermodynamics kinetics and species transport processes. However, due to the high temperature at the interface, the chemical kinetics rate is swift. Therefore, the limiting factor is the species transport process in steel and slag [8], [13], [14], [26]. Namely, the desulfurization rate is controlled by the species transfer rate in the steel and the slag.

In the steel phase, the species transport is enhanced by the argon stirring effect, and the species exchange between slag and steel is promoted. In order to indicate the transfer rate, the mass transfer coefficient of species i in steel, $k_{m,\mathrm{i}}$, and mass transfer coefficient of species i in slag, $k_{s,\mathrm{i}}$. There are several empirical expressions proposed to calculate the overall mass transfer coefficient in steel based on boundary conditions and other operating parameters [13], [28]. However, they are suitable for most mathematical models because the local sulfur distribution is not investigated but not appropriate for CFD models since the local mass transfer effect at the interface is not studied. Instead of adopting the empirical formulas, Lou [14] adopts the Kolmogorov theory of isotropic turbulence [14] to calculate $k_{m,\mathrm{i}}$ as shown below :

$$k_{m,\mathrm{i}} = cD_{m,\mathrm{i}}^{0.5}\left(\frac{\varepsilon_l}{\nu}\right)^{0.25} \tag{2.46}$$

$$k_{s,\mathrm{i}} = cD_{s,\mathrm{i}}^{0.5}\left(\frac{\varepsilon_l}{\nu}\right)^{0.25} \tag{2.47}$$

where c is a constant and is 0.4 for this study [29]; $D_{m,\mathrm{i}}$ and $D_{s,\mathrm{i}}$ stand for the diffusion coefficient of species i in steel and slag, which are assumed to be uniform values of 7.0×10^{-9} m^2/s and 7.0×10^{-11} m^2/s, respectively. ε_l is the local turbulent energy dissipation rate calculated by ANSYS Fluent and ν is the kinematic viscosity of steel phase. Therefore, the mass transfer coefficient $k_{m,\mathrm{i}}$ is the same for each species in steel phase, and $k_{s,\mathrm{i}} = 0.1k_{m,\mathrm{i}}$.

2.2.3 Species Transfer Rate

In the steel phase, the dissolved sulfur is carried by the flow towards the slag-steel interface, where it reacts with lime from slag and the CaS is composed and absorbed by slag, as described in Equation 2.36. The sulfur molar flux from steel to the interface can be written as follows:

$$J_{m,S} = \frac{k_{m,S}\rho_m}{100M_S}\left\{[\%-S]-[\%-S]^*\right\} \tag{2.48}$$

where $k_{m,S}$ is the mass transfer coefficient of sulfur in steel as shown in Equation 2.46; ρ_m is the steel density; M_S is the molecular mass of sulfur; $[\%-S]$ and $[\%-S]^*$ represent the local sulfur mass fraction and mass fraction of sulfur at equilibrium, respectively.

Simultaneously, the mole flux of CaS from the interface to the slag can be obtained by the following equation:

$$J_{s,CaS} = \frac{k_{s,CaS}\rho_s}{100M_{CaS}}\{(\%-CaS)-(\%-CaS)^*\} \tag{2.49}$$

where $k_{s,CaS}$ is the mass transfer coefficient of CaS in slag as shown in Equation 2.47; ρ_s is the slag density; M_{CaS} is the molecular mass of CaS; $(\%-CaS)$ and $(\%-CaS)^*$ represent the local CaS mass fraction and mass fraction of CaS at equilibrium, respectively. However, instead of monitoring the CaS mole flux, we can focus on the sulfur mole flux from the interface to the slag phase. Therefore, the Equation 2.49 can be written as follows:

$$J_{s,CaS} = J_{s,S} = \frac{k_{s,S}\rho_s}{100M_S}\{(\%-S)-(\%-S)^*\} \tag{2.50}$$

According to stoichiometric balance, the mole flux of sulfur from steel towards the interface equals to the mole flux of sulfur from the interface to the slag[13]:

$$J_{m,S} = J_{s,S} \tag{2.51}$$

By combining Equation 2.38, Equation 2.48, and Equation 2.50, the following expression for the equilibrium sulfur mass fraction in steel $[\%-S]^*$ is obtained:

$$[\%-S]^* = \frac{k_m\rho_m[\%-S]+k_S\rho_S(\%-S)}{k_m\rho_m+k_s\rho_s L_S} \tag{2.52}$$

Therefore, by introducing Equation 2.52 to the Equation 2.48, the sulfur mole flux can be written as follows:

$$J_S = \frac{\rho_m}{100M_S}k_{eff,S}\left\{[\%-S]-\frac{(\%-S)}{L_S}\right\} \tag{2.53}$$

$$k_{eff,S} = \frac{\rho_s k_{m,S}k_{s,S}L_S}{k_{m,S}\rho_m+\rho_s k_{s,S}L_S} \tag{2.54}$$

where $k_{eff,S}$ is the overall mass transfer coefficient of sulfur between slag and steel.

Since the chemical reaction rate is controlled by species transport process, the mole flux of sulfur in Equation 2.53 indicates the desulfurization rate during the secondary steelmaking stage. However, to introduce the sulfur transport rate, the source term of sulfur is required[30], which is obtained based on the sulfur mole flux and can be written as follows:

$$S_S = \frac{\rho_m A}{100V} k_{eff,S} \left\{ [\%-S] - \frac{(\%-S)}{L_S} \right\} \tag{2.55}$$

where A is the local interface area based on the mesh size and V is the cell volume of the steel phase at the slag-steel interface zone.

2.3 Simulation Conditions and Procedures

In this study, the chemical reaction process is investigated by the commercial CFD software ANSYS Fluent to simulate the flow field of liquid steel during the secondary steelmaking process and the change of species mass fraction. The user-defined functions are used to describe the chemical reaction rate. A full-scale ladle model developed based on a simplified Nucor ladle is used in this study.

2.3.1 Computational Geometry

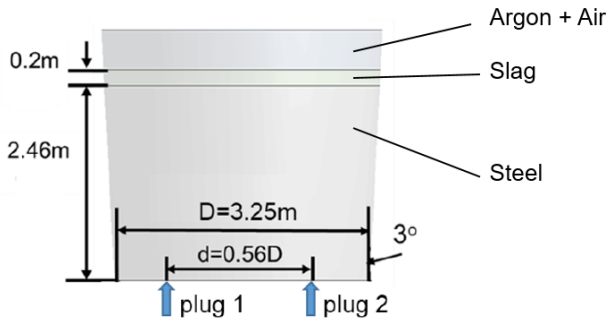

Figure 2.1. Schematic diagram of simplified ladle.

As shown in Figure 2.1, there are three computational domains: steel domain, slag domain, and air domain. The height of the steel domain is 2.46 m, and the thickness of the

slag is 0.2 m. The size of the air layer above the slag layer is not a critical parameter in this model as long as the steel phase does not reach the top surface, and the thickness of air layer is 0.5 m in this study. There are two plugs at the bottom of the ladle where the argon gas is injected into the steel. The diameter of bottom surface D is 3.25 m, and the difference between two plugs is $0.56D$. In this study, two kinds of ladles with different plug separation angles are investigated: 180° separation ladle and 90° separation ladle, as shown in Figure 2.2.

(a) (b)

Figure 2.2. Schematic diagram of different plug separation angles: (a) 90°; (b) 180°.

2.3.2 Mesh and Boundary Conditions

The mesh of the 90° ladle is shown in Figure 2.3. There is finer mesh at the slag-steel interface, the slag-argon interface, and the inlet surface and bubble-liquid plume zone. There are two types of boundary conditions: the top surface is treated as a pressure-outlet with steel phase backflow so that the steel can remain in the domain. The other boundaries are set to be the no-slip wall. For the discrete bubble particle, the surface injection release method is used at the plug area. The top surface is considered to be the escape type to make argon leave the domain. The type of other boundaries is reflect for the discrete phase.

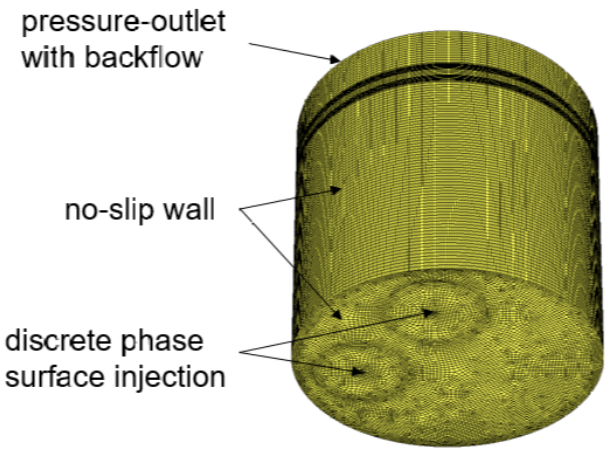

Figure 2.3. Schematic diagram of mesh.

2.3.3 Initial Conditions

The parameters employed in the model are listed in Table 2.3. In this study, there are two argon gas flow rate: 5 SCFM and 20 SCFM. Combining with the plug separation angles and argon flow rate, there are 4 scenarios investigated in this study to find out their effects on desulfurization rate: (1) 90° separation angle with 5 SCFM flow rate for both plugs; (2)180° separation angle with 5 SCFM flow rate for both plugs; (3) 90° separation angle with 5 SCFM flow rate for one plug and 20 SCFM for another plug; (4) 90° separation angle with 20 SCFM flow rate for both plugs. The initial compositions in steel and slag are selected form a typical scenario [14] and are summarized in Table 2.4. The temperature in the ladle, including both steel phase and slag phase, is assigned to be 1833 K and the temperature gradient and variation during the secondary steelmaking process can be ignored.

2.3.4 Simulation Procedure

The simulation is split into two parts. The multiphase flow field is derived in the first step in each scenario in the quasi-steady state. The slag-steel interface's shape and the slag eye's size are evaluated, and the slag phase and the argon phase are removed from the computational domain. The second step uses source terms computed from user-defined functions to

Table 2.3. Parameters employed in the CFD simulation

Density of steel	6975 kg/m^3
Density of slag	2786 kg/m^3
Density of argon	0.719 kg/m^3
Viscosity of steel	0.006 kg/(m-s)
Viscosity of slag	0.06 kg/(m-s)
Viscosity of argon	2.125×10^{-5} kg/(m-s)
Surface tension coefficient between steel and slag	1.15 N/m
Surface tension coefficient between steel and argon	1.823 N/m
Argon flow rate of each plug	5 SCFM, 20 SCFM

Table 2.4. Initial chemical composition of steel and slag

	Steel composition (%)
S	0.0107
Al	0.058
Mn	0.66
Si	0.18
C	0.35
	Slag composition (%)
Al_2O_3	21.32
MnO	0.24
SiO_2	5.84
CaO	57.79
MgO	6.02
FeO	0.95
S	0.07

explore the desulfurization process in the updated steel phase computational domain. The species concentration in slag is assumed to be uniform and numerically determined using particular formulas from user-defined functions for the species mass fraction variety in the slag phase [14].

The slag-steel interface is assigned to be the degassing boundary condition so that only the argon phase can escape from the interface while the steel phase remains in the computational domain[30]. The velocity-inlet is used at each plug. Other boundaries are set to be the no-slip solid wall with standard wall function to model the near-wall region.

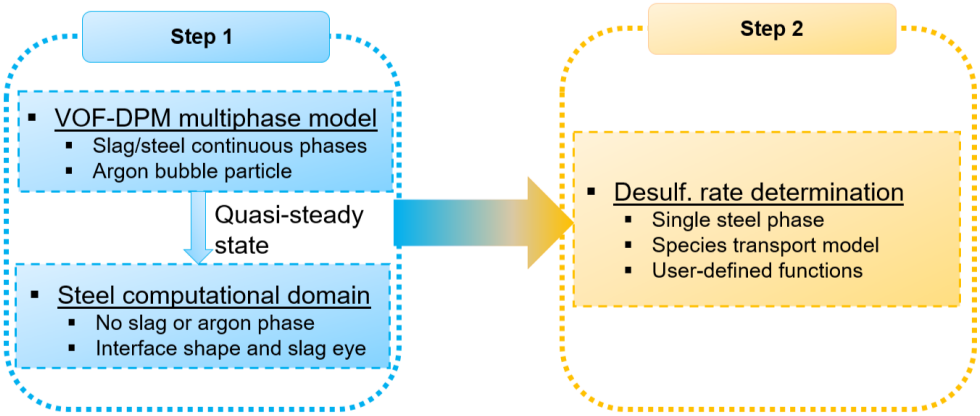

Figure 2.4. Desulfurization simulation procedure.

3. RESULT AND DISCUSSION

In this chapter, both the VOF-DPM multiphase flow part and desulfurization rate determination part are proved to accurately simulate the slag-steel interface area and sulfur mass fraction variety with time compared to industrial measurement, respectively. Based on a Nucor generic ladle, the flow field and desulfurization process are computed in different scenarios by this CFD model to investigate the influence of stirring conditions on the sulfur removal rate and, therefore, to optimize the ladle design for lower sulfur content.

3.1 CFD Model Validation

A plant trial is obtained in a Nucor generic ladle during a practical procedure where the plug separation angle is 180° and argon flow rate for each plug is 30 SCFM, and the result shows the slag eye diameter is 0.73 m. Based on the multiphase flow model above under the same plug arrangement and argon flow rate conditions, the predicated slag eye diameter at a quasi-steady state is 0.79 m. The overall percentage error of 7.5% compared to industrial measurement, indicating that the simulation result match well with the plant trial, and therefore the VOF-DPM multiphase model can estimate the steel/slag/argon multiphase flow in a Nocur generic ladle.

The desulfurization rate determination section has undergone validation. An 80-ton ladle has been used to investigate the desulfurization process. The sulfur mass fraction is estimated using the model proposed in this study under identical treatment settings. The simulation result shows excellent agreement with both industrial measurements and simulation predictions from Lou's work [14] using (Al_2O_3)-(FeO)-(SiO_2)-(MnO)-[O]-[S] equilibrium approach shown in Figure 3.1. The maximum sulfur mass fraction error between simulation and measurement during the entire treatment is 5.8 %, demonstrating that the desulfurization rate determination model based on [Al]-[O]-(Al_2O_3) equilibrium approach can predict the sulfur removal process in a gas-stirred ladle.

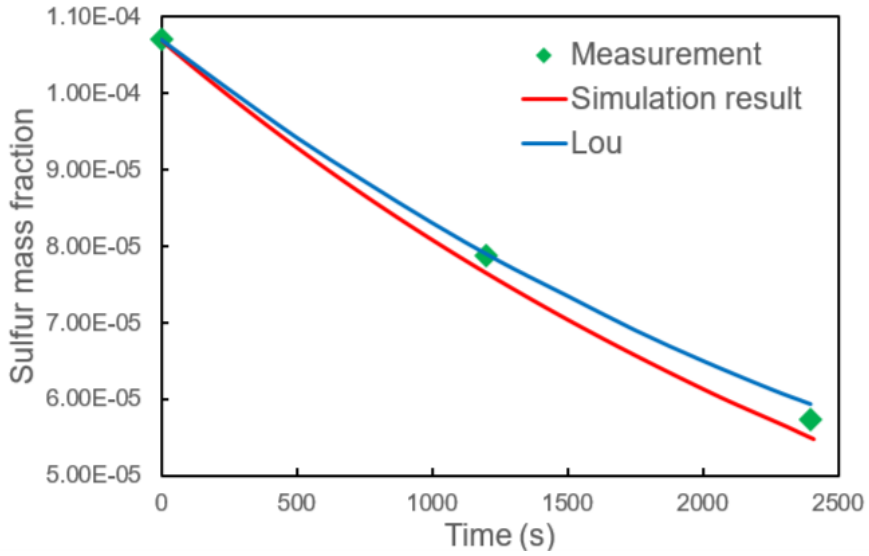

Figure 3.1. Sulfur mass fraction with time in the validation study.

3.2 Steel Computational Domain

The slag-steel interface at quasi-steady state is tracked by the VOF-DPM multiphase model in each scenario shown in Figure 3.2. It can be seen that there is no slag eye at the interface above each plume in the 90°-5/5 SCFM scenario and the 180°-5/5 SCFM scenario. In the 90°-5/20 SCFM scenario, a slag eye exits above the 20 SCFM gas plume while two slag eyes are formed at the interface in the 90°-20/20 SCFM scenario. The interface shapes and slag eye position and size are recorded in the steel phase, treated as the desulfurization simulation computational domain. The interface is not a flat surface but with some extrusions on it, as shown in Figure 3.3. For the most part, the bump exists above each bubble plume, but it is hard to observe one overhead the 5 SCFM plume in the 90°-5/20 SCFM scenario. Then the species transport model is introduced to this updated single-phase domain to predicate the sulfur transfer process in steel, and the desulfurization rate determination part is added to the model to calculate the sulfur removal rate at the interface. The slag and air phases are removed from the computational domain and are no longer simulated in the following desulfurization study.

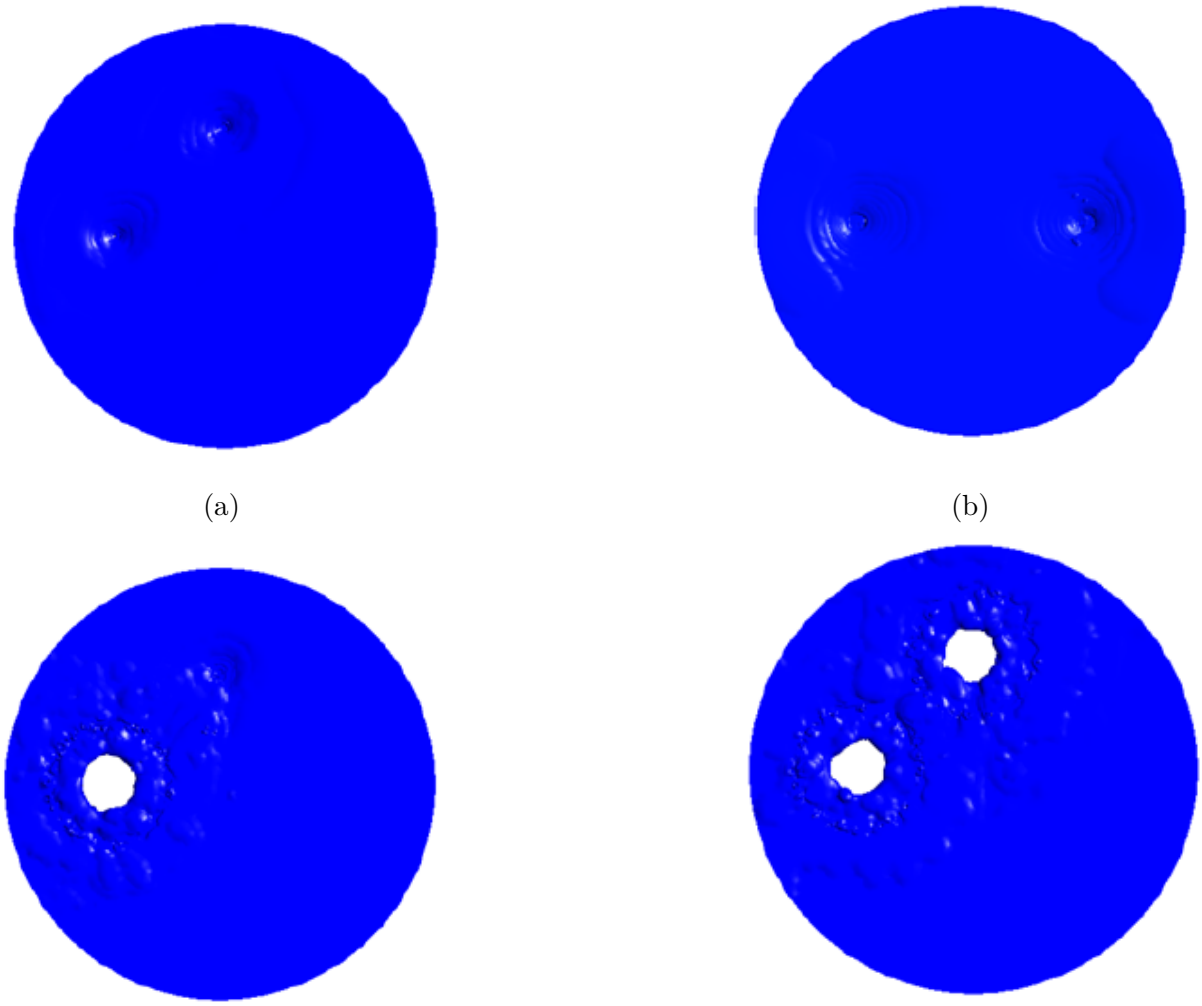

(a) (b)

(c) (d)

Figure 3.2. Predicated slag-steel interface of different scenarios in quasi-steady state : (a) 90° 5/5 SCFM; (b) 180° 5/5 SCFM; (c) 90° 5/20 SCFM; (d) 90° 20/20 SCFM.

3.3 Simulation Results

3.3.1 Flow Field and Mass Transfer Coefficient

Figure 3.4 depicts the steel velocity of various scenarios in the equilibrium condition. Steel velocity is high at the plug zones under the influence of argon stirring and gradually diminishes along each argon-bubble plume from the bottom to the interface. However, the steel velocity is very low at the bump region of the interface, indicating that the slag layer

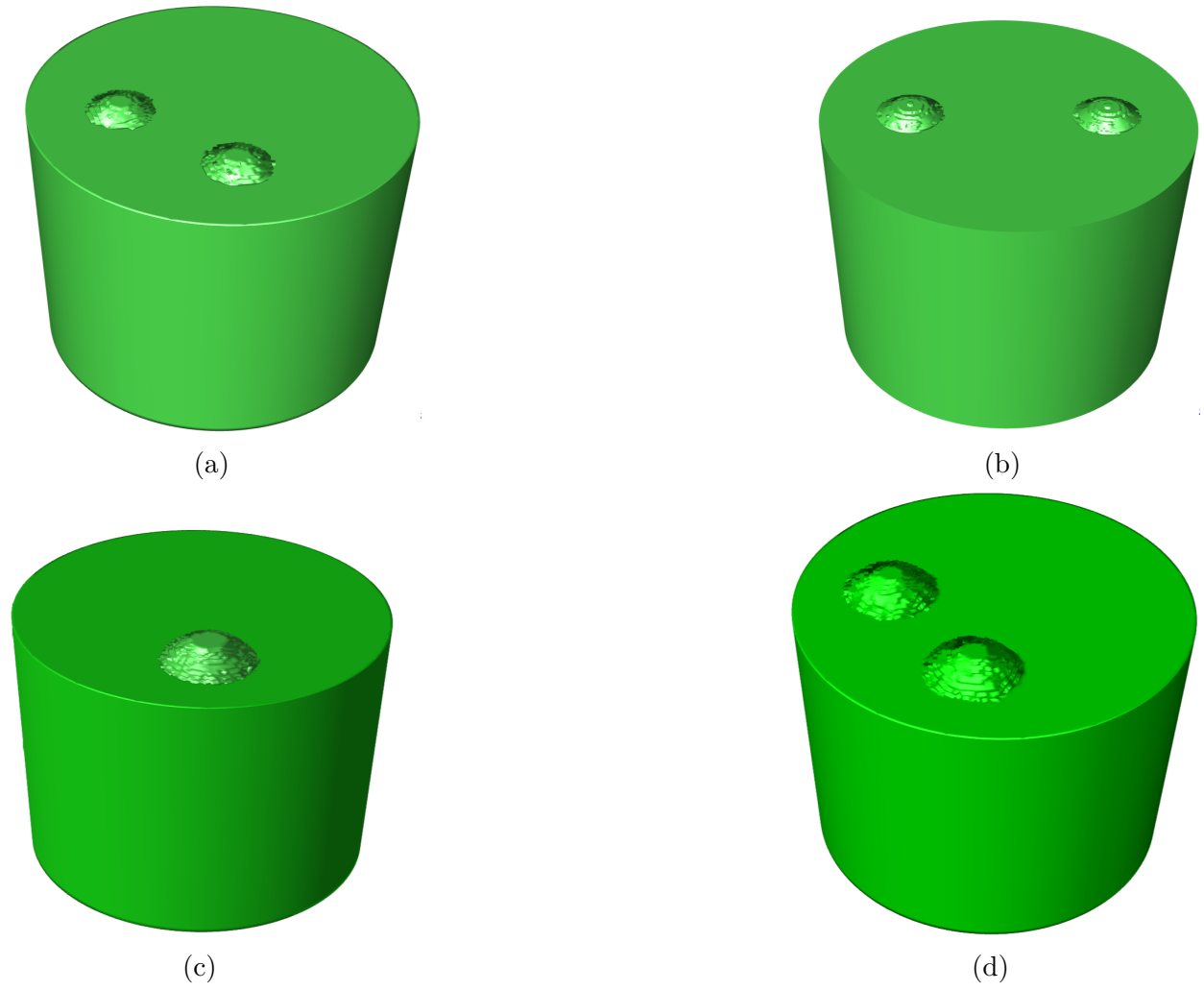

Figure 3.3. Steel phase computational domain of different scenarios in quasi-steady state : (a) 90° 5/5 SCFM; (b) 180° 5/5 SCFM; (c) 90° 5/20 SCFM; (d) 90° 20/20 SCFM.

impairs the vertical flow, and the kinetic energy is utilized to promote slag layer deformation and the development of slag eyes. In the 90°-5/20 SCFM scenario, the argon-bubble plume of 5 SCFM bends and moves to the 20 SCFM plume during the ascent, consuming the longitudinal kinetic energy. Therefore, there is no visible bulge when the 5 SCFM plume hits the interface.

Figure 3.5 shows the steel turbulent dissipation rates under various situations. The turbulent dissipation rate is significant at the plug area and then drops along the agron-bubble plume, similar to the velocity distribution in the steel domain. Nonetheless, the

dissipation rate in the bump zones at the interface is high. The turbulent dissipation rate climbs somewhat from the center of the bump to the edge of the bump, then steadily decreases to the sidewall.

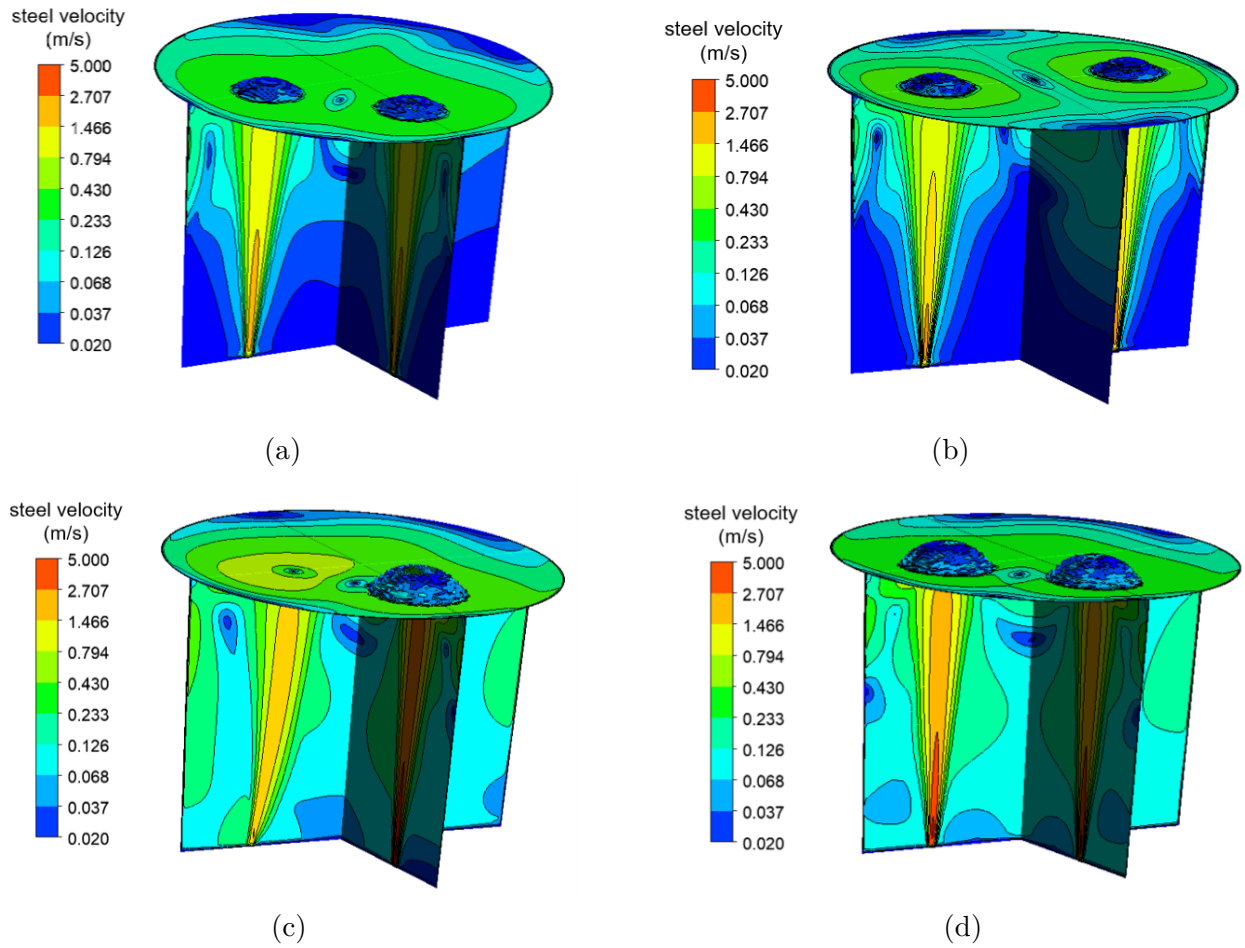

Figure 3.4. Steel velocity of different scenarios in quasi-steady state : (a) 90° 5/5 SCFM; (b) 180° 5/5 SCFM; (c) 90° 5/20 SCFM; (d) 90° 20/20 SCFM.

Figure 3.6 demonstrates the mass transfer coefficient k_m at the slag-steel interface. The local k_m distribution at the interface is notably similar to the turbulent dissipation rate: From the center of the bump to the edge of the bump, k_m gently rises and afterward starts decreasing until it reaches the sidewall, which is because the k_m is proportional to the steel turbulent dissipation rate as specified in Equation 2.46.

Table 3.1 displays the average k_m values at the slag-steel interface for various circumstances. When the plug separation angle is adjusted from 90° to 180°, the average k_m

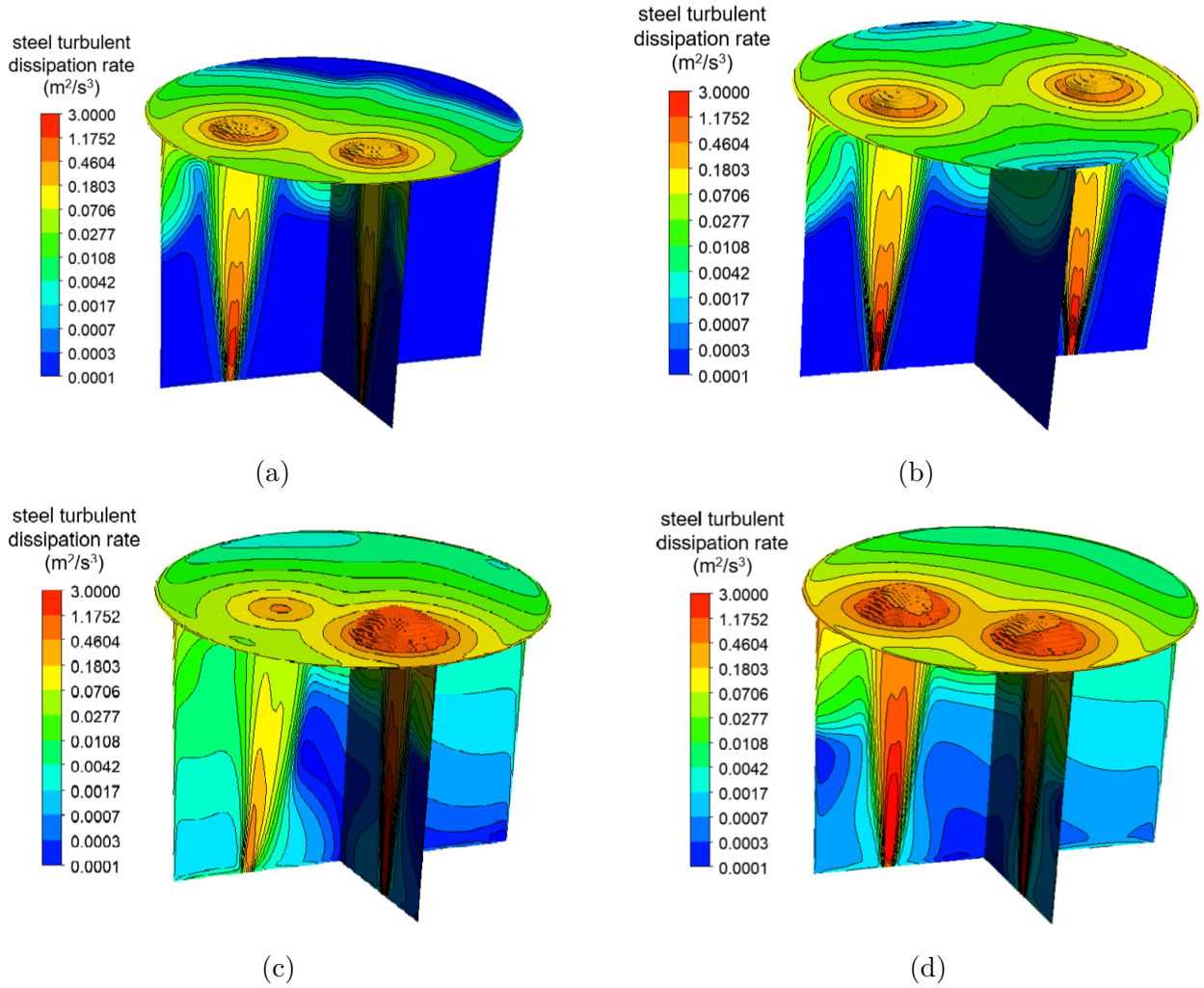

Figure 3.5. Steel turbulent dissipation rate of different scenarios in quasi-steady state : (a) 90° 5/5 SCFM; (b) 180° 5/5 SCFM; (c) 90° 5/20 SCFM; (d) 90° 20/20 SCFM.

marginally rises, indicating that the species transport process from the steel to the slag-steel interface is improved. When the separation angel remains constant at 90°, a higher argon flow rate results in a bigger average k_m: when the argon flow rate rises from 5/5 SCFM to 5/20 SCFM, the k_m value rises by 24.86 %, and when the argon flow rate increases from 5/5 SCFM to 20/20 SCFM, the k_m value rises by 47.06 %. The 90°-20/20 SCFM has the highest average k_m of all scenarios at the slag-steel interface, indicating that the mass transport rate is the largest in this scenario.

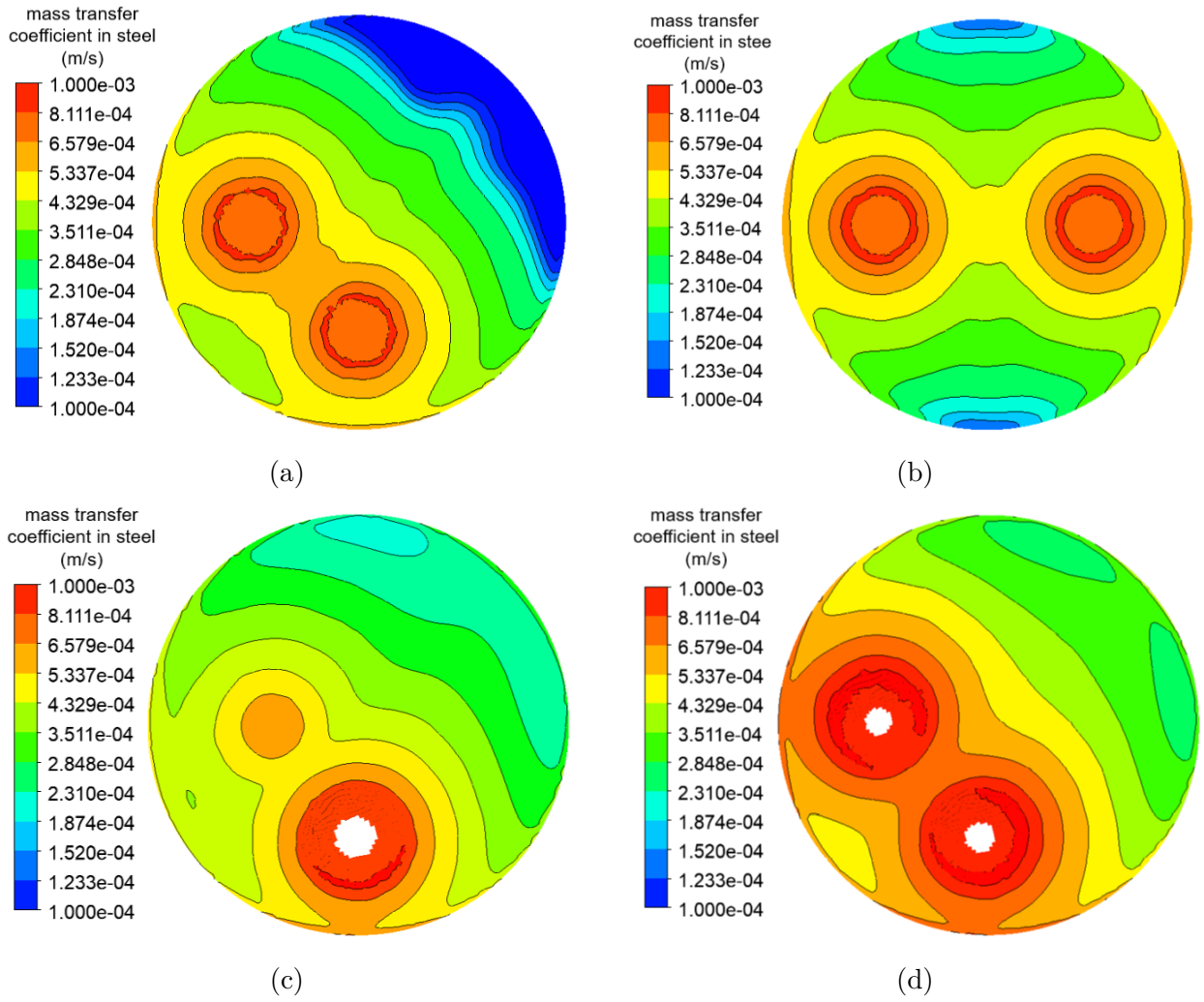

Figure 3.6. Mass transfer coefficient of species in steel phase of different scenarios in quasi-steady state : (a) 90° 5/5 SCFM; (b) 180° 5/5 SCFM; (c) 90° 5/20 SCFM; (d) 90° 20/20 SCFM.

3.3.2 Effect of Ladle Design on Desulfurization Rate

The sulfur removal process is explored by introducing the species transport model and source terms derived by user-defined functions to the computational domain after getting the steel flow field and mass transfer coefficient in each scenario. Figure 3.7 exhibits the sulfur mass fraction variation in different scenarios after 10 minutes of treatment. In each scenario, the sulfur mass fraction falls over time, demonstrating that sulfur is transferred from the steel phase to the slag phase during secondary steelmaking. In each scenario, the

Table 3.1. Average k_m on slag-steel interface in different scenarios

Scenario	Average k_m ($m \cdot s^{-1}$)
90° 5/5 SCFM	4.131×10^{-4}
180° 5/5 SCFM	4.216×10^{-4}
90° 5/20 SCFM	5.158×10^{-4}
90° 20/20 SCFM	6.075×10^{-4}

ultimate sulfur content is different. In the 90°-5/5 SCFM scenario, the sulfur mass fraction drops from 1.07×10^{-2} % to 9.70×10^{-3} % after 10 minutes, whereas the steel has 9.66×10^{-3} % sulfur in the 180°-5/5 SCFM scenario at the end of the treatment. The eventual sulfur content is 9.55×10^{-3} % and 9.38×10^{-3} % in the 90°-5/20 SCFM scenario and 90°-20/20 SCFM scenario, respectively.

Table 3.2 calculates and summarizes the average desulfurization rate in each scenario. In the 90°-5/5 SCFM scenario, the average desulfurization rate is 1.66×10^{-4} % per second. The sulfur removal rate increases by 4.82 % when the plug separation angle is adjusted from 90° to 180°. When the argon flow rate is increased from 5/5 SCFM to 5/20 SCFM under the same plug separation angle of 90°, the sulfur exchange rate goes up to 1.92×10^{-4} % per second, an increase of 15.66 %; when using 20/20 SCFM argon flow rate, the reaction rate increases to 2.20×10^{-4} % per second, a growth of 32.53 % over the 5/5 SCFM gas stirring condition. Therefore, the ladle structure and stirring conditions can affect the desulfurization rate in secondary steelmaking: a ladle with 180° plug separation angle has better desulfurization behaviors than a ladle with 90° plug separation angle; a higher argon flow rate can accelerate the sulfur removal process.

When comparing Table 3.1 and Table 3.2, it can be seen that the sequence of average desulfurization rate in each scenario is the same as the sequence of k_m: the k_m and desulfurization rate in the 90°-20/20 SCFM scenario are the highest, followed by the 90°-5/20 SCFM scenario and the 180°-5/5 SCFM scenario; the k_m and desulfurization rate in the 90°-5/5 SCFM scenario are the lowest. Thereby, the k_m appears to have a significant influence on the desulfurization process.

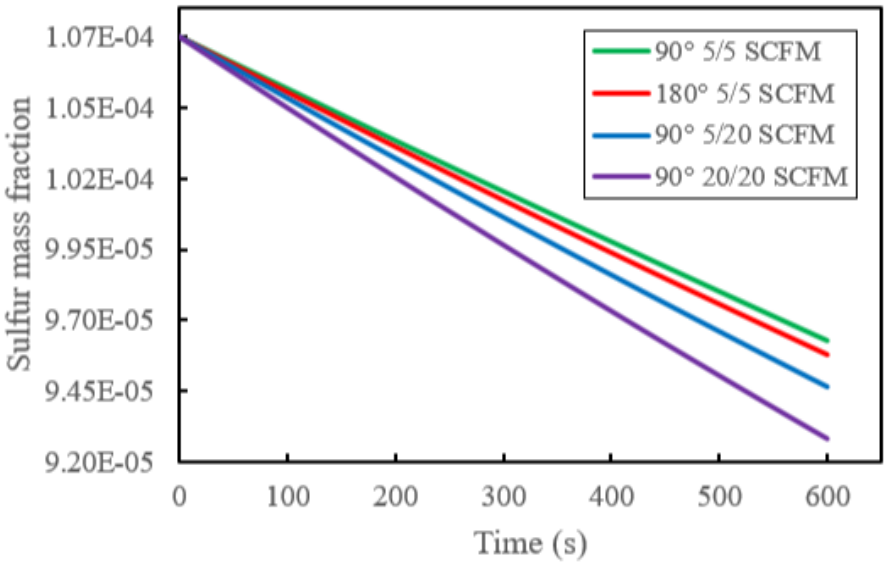

Figure 3.7. Sulfur mass fraction in different scenarios.

Table 3.2. Average desulfurization rate in different scenarios

Scenario	Average rate (%/s)
90° 5/5 SCFM	1.66×10^{-4}
180° 5/5 SCFM	1.74×10^{-4}
90° 5/20 SCFM	1.92×10^{-4}
90° 20/20 SCFM	2.20×10^{-4}

Figure 3.8 depicts the transient sulfur molar flux at the interface described in Equation 3.8 after 300 seconds from the start of the treatment to display the local desulfurization rate. Overall, the sulfur molar flux is high at the bump zones at the interface where the argon-bubble plume contacts the slag layer, signifying a strong desulfurization rate in these areas, and then it progressively declines towards the sidewall. Based on a comparison between Figure 3.6 and Figure 3.8, the sulfur molar flux distribution at the interface is similar to the k_m distribution in each scenario. As a result, the k_m at the interface can, to some extent, dictate the desulfurization rate at the interface.

Figures 3.9 to Figure 3.12 illustrate the transient sulfur molar flux at the interface in 100 seconds, 300 seconds, and 600 seconds after the start of treatment under 90°-5/5 SCFM scenario, 180°-5/5 SCFM scenario, 90°-5/20 SCFM scenario, and 90°-20/20 SCFM scenario,

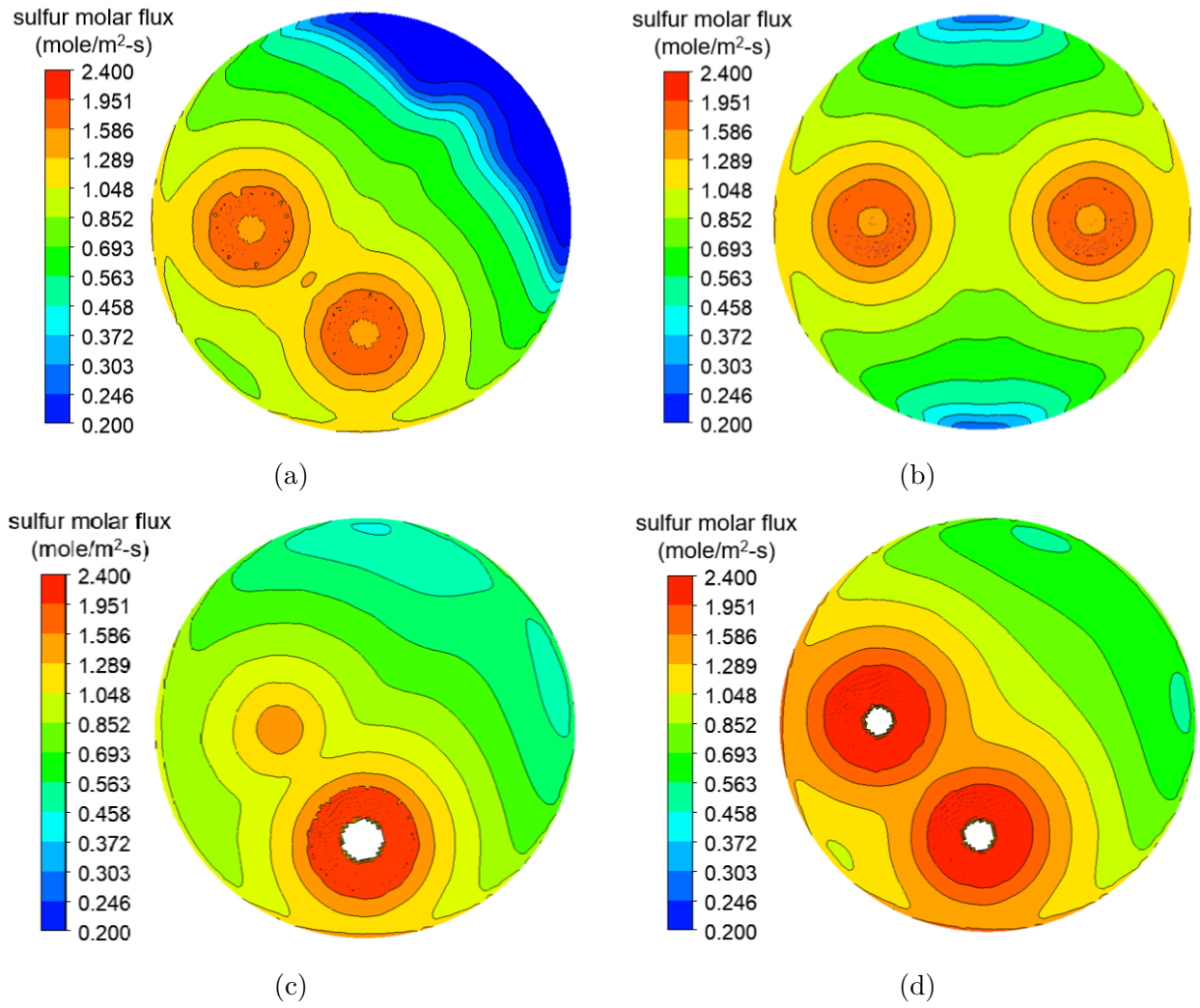

Figure 3.8. Transient sulfur molar flux at the slag-steel interface after 300 seconds treatment in different scenarios : (a) 90° 5/5 SCFM; (b) 180° 5/5 SCFM; (c) 90° 5/20 SCFM; (d) 90° 20/20 SCFM.

respectively. In each case, the sulfur molar fluxes at the interface decrease somewhat with time, suggesting that desulfurization slows down during the treatment. It demonstrates that desulfurization efficiency diminishes with time under specific stirring conditions and that this problem cannot be overcome by optimizing ladle construction or adjusting the argon flow rate.

From Figure 3.13 to Figure 3.16, the values of oxygen activity a_O at the slag-steel interface in 200 seconds, 300 seconds, and 400 seconds after the start of argon blowing are presented,

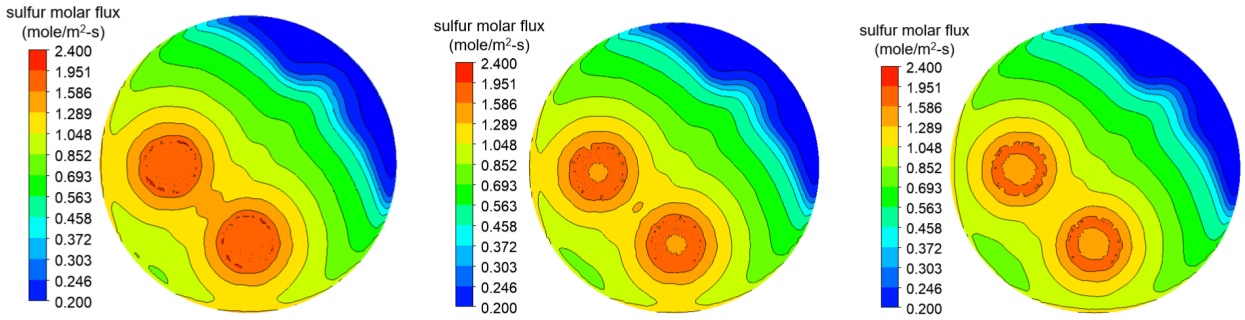

Figure 3.9. Transient sulfur molar flux at the slag-steel interface after different time of treatment in 90°-5/5 SCFM scenario : (a) 100 s; (b) 300 s; (c) 600 s.

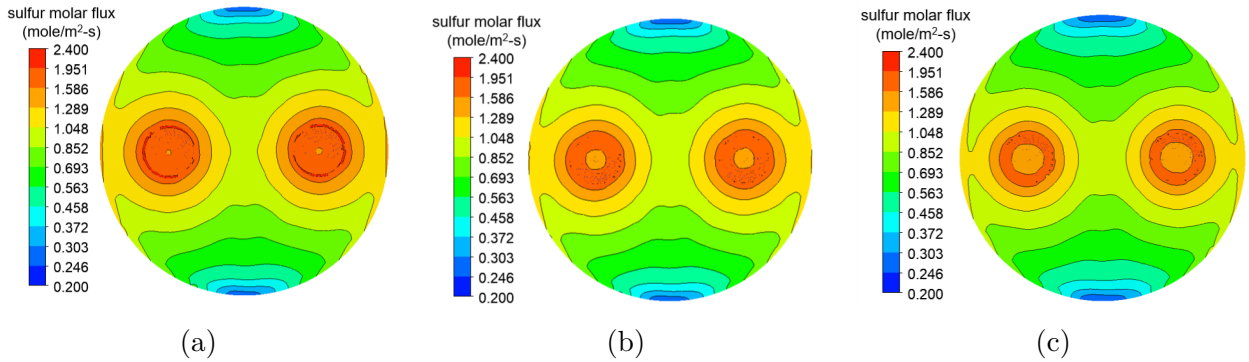

Figure 3.10. Transient sulfur molar flux at the slag-steel interface after different time of treatment in 180°-5/5 SCFM scenario : (a) 100 s; (b) 300 s; (c) 600 s.

respectively, for the 90°-5/5 SCFM scenario, 180°-5/5 SCFM scenario, 90°-5/20 SCFM scenario, and 90°-20/20 SCFM scenario. In general, in each scenario, the oxygen activity at the interface increases over time. A larger a_O results in a decreased sulfur distribution ratio L_S, according to Equation 2.38. As a result, during secondary steelmaking, the L_S at the interface decreases. Because the k_m and k_s do not vary with time in a quasi-steady flow field, the overall mass transfer coefficient k_{eff} in Equation 2.54 declines with L_S reduction. As previously stated, sulfur is removed from the steel and absorbed by the slag, resulting in a decrease in $[\% - S]$ while an increase in $(\% - S)$ over time. Thereby, the value of the term $[\% - S] - \frac{(\% - S)}{L_S}$ in Equation 2.53 gets less and less. As a result, as illustrated in Figures 3.9

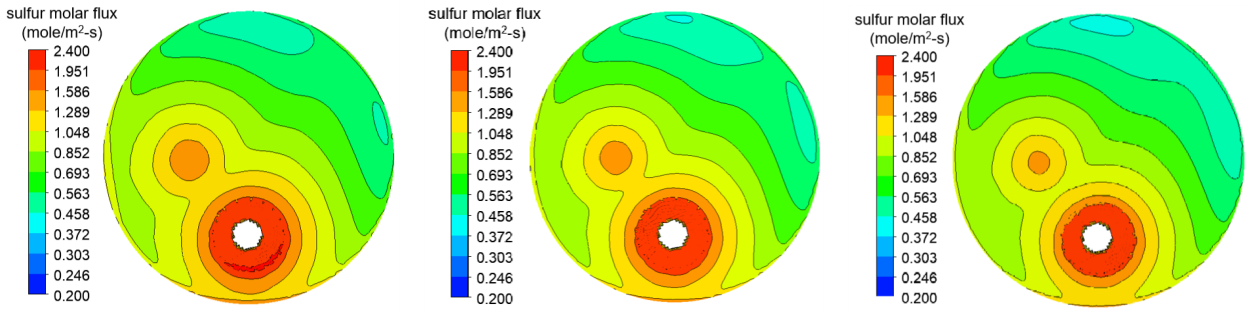

Figure 3.11. Transient sulfur molar flux at the slag-steel interface after different time of treatment in 90°-5/20 SCFM scenario : (a) 100 s; (b) 300 s; (c) 600 s.

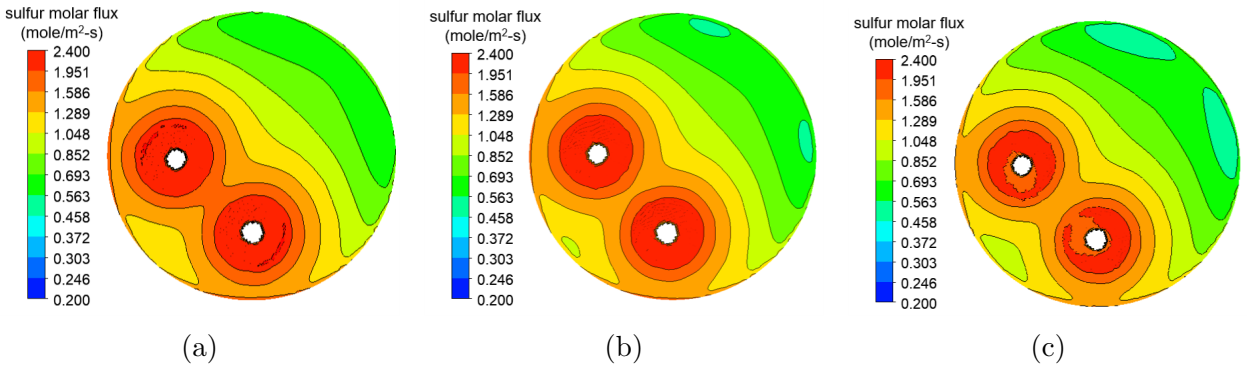

Figure 3.12. Transient sulfur molar flux at the slag-steel interface after different time of treatment in 90°-5/5 SCFM scenario : (a) 100 s; (b) 300 s; (c) 600 s.

to Figure 3.12, the sulfur molar flow at the interface is reduced in each scenario. Thus, the a_O growth rate should be managed to maintain the desulfurization rate and remove more sulfur from the steel under particular operating conditions.

The a_O distribution patterns can also be observed at a certain point in each scenario: the a_O is small at the bump zones at the interface and continuously rises towards the sidewall. As explained previously, a bigger a_O results in a lower desulfurization rate. Based on the a_O distribution patterns and the relationship between a_O and sulfur molar flux, it can be estimated that the desulfurization rate is low near the sidewall and high in the bump zones, as illustrated from Figures 3.9 to Figure 3.12. However, the desulfurization rate distribu-

tion patterns are closer to the k_m distribution patterns than the a_O distribution contours. Consequently, the k_m has a greater impact on the desulfurization rate in this study than the a_O.

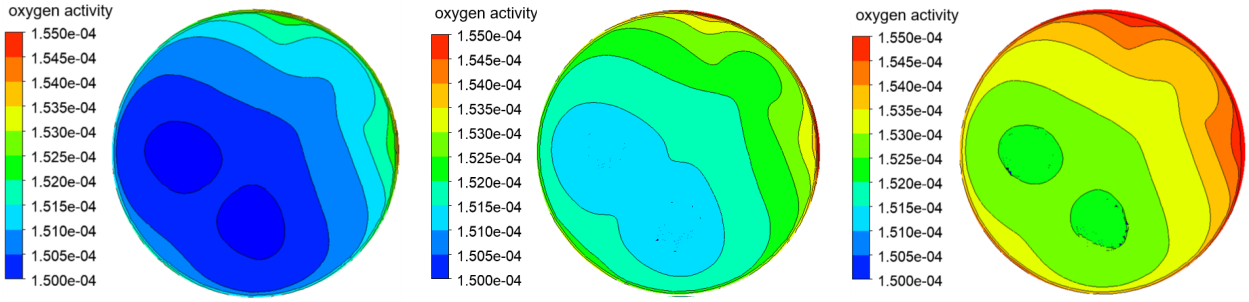

(a) (b) (c)

Figure 3.13. Oxygen activity at the slag-steel interface after different time of treatment in 90°-5/5 SCFM scenario : (a) 200 s; (b) 300 s; (c) 400 s.

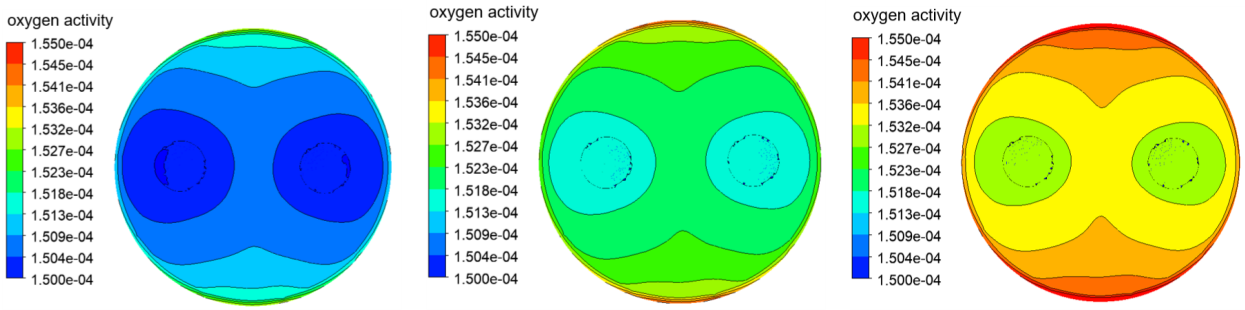

(a) (b) (c)

Figure 3.14. Oxygen activity at the slag-steel interface after different time of treatment in 180°-5/5 SCFM scenario : (a) 200 s; (b) 300 s; (c) 400 s.

Figures 3.17 to Figure 3.20 depict the distribution of sulfur content in 100 seconds, 300 seconds, and 600 seconds after the desulfurization process started in each scenario. The sulfur concentration in the steel domain clearly reduces over time. Compared to other zones in the domain, the sulfur mass percentage is more significant in the argon-bubble plume area. The sulfur mass fraction is prominent at the bottom of the ladle in both the 90°-5/5 SCFM and 180°-5/5 SCFM scenarios, and it steadily decreases along the streamline from the plug to the interface. The sulfur mass fraction gradient along the streamline in the argon-bubble

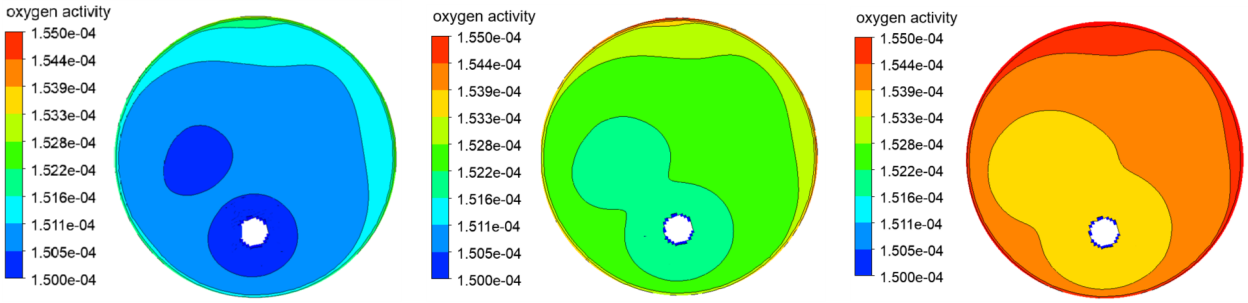

(a) (b) (c)

Figure 3.15. Oxygen activity at the slag-steel interface after different time of treatment in 90°-5/20 SCFM scenario : (a) 200 s; (b) 300 s; (c) 400 s.

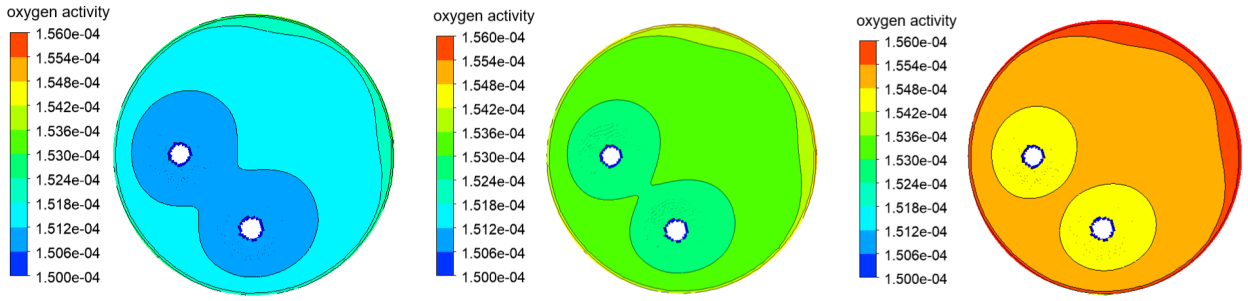

(a) (b) (c)

Figure 3.16. Oxygen activity at the slag-steel interface after different time of treatment in 90°-20/20 SCFM scenario : (a) 200 s; (b) 300 s; (c) 400 s.

plume is not as noticeable in the 90°-5/20 SCFM and 90°-20/20 SCFM scenarios, indicating that the sulfur distribution is more even, which could be due to the more substantial mixing effect with a high argon flow rate. In each scenario, the sulfur concentration is highest in the extruded zones at the interface and subsequently decreases along the streamline until it reaches the sidewalls. One possible explanation for this phenomenon is that sulfur is carried to the bump zones by liquid flow stirred by argon gas, resulting in a high sulfur concentration; then sulfur is gradually removed from the steel due to desulfurization as sulfur moves along the streamline, lowering the sulfur content at the interface. Although the rate of desulfurization is higher in the bumps than in other areas of the interface, as stated previously, the sulfur concentration in the bump areas remains significant. Thus, the sulfur removal process detailed in Equation 2.53 is slower than the sulfur supplement

process carried out by the flow in the steel domain, and the terms in Equation 2.53 are limiting factors of the desulfurization in this study.

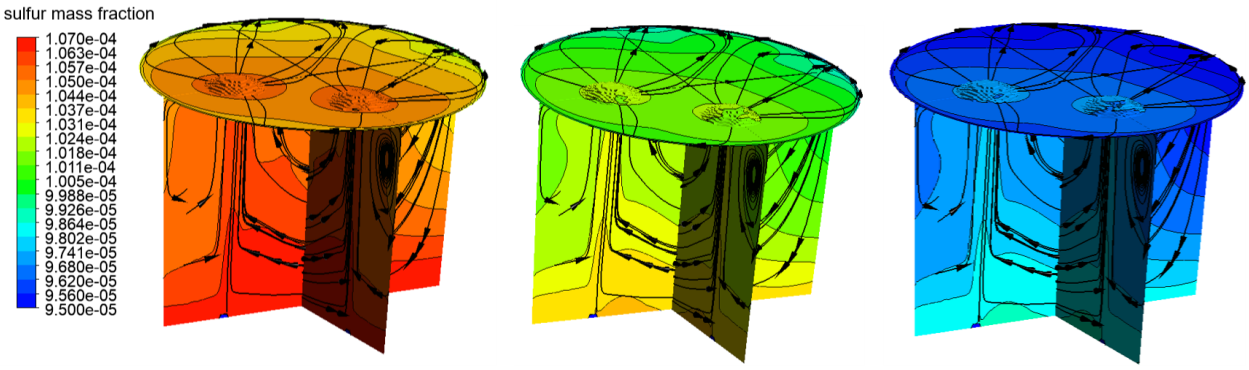

(a) (b) (c)

Figure 3.17. Sulfur content distribution at different time in the 90°-5/5 SCFM scenario : (a) 100 s; (b) 300 s; (c) 600 s.

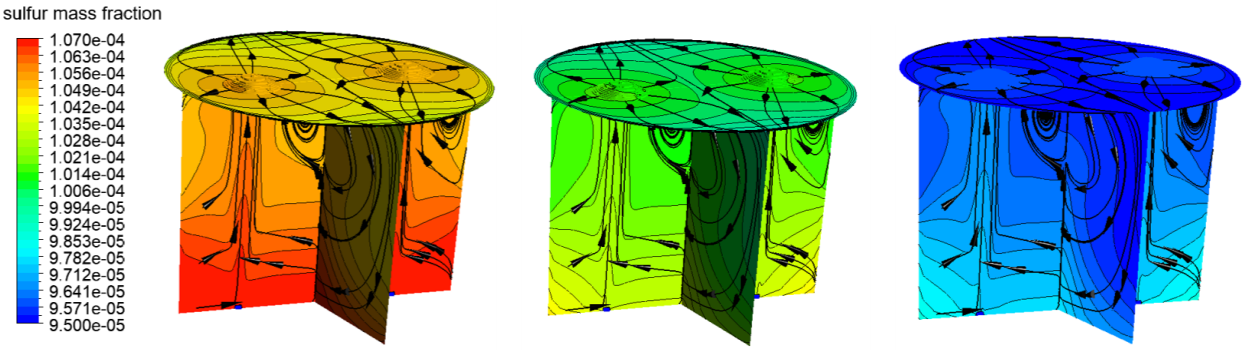

(a) (b) (c)

Figure 3.18. Sulfur content distribution at different time in the 180°-5/5 SCFM scenario : (a) 100 s; (b) 300 s; (c) 600 s.

3.3.3 Effect of Steel Temperature on Desulfurization Rate

It is estimated that the temperature may drop about 60 K to 100 K during the refining process without reheating treatment. According to Equation 2.44, the steel temperature impacts oxygen activity. Therefore, the temperature change probably affects the desulfurization rate. In order to explore the impacts of temperature on desulfurization rate, three

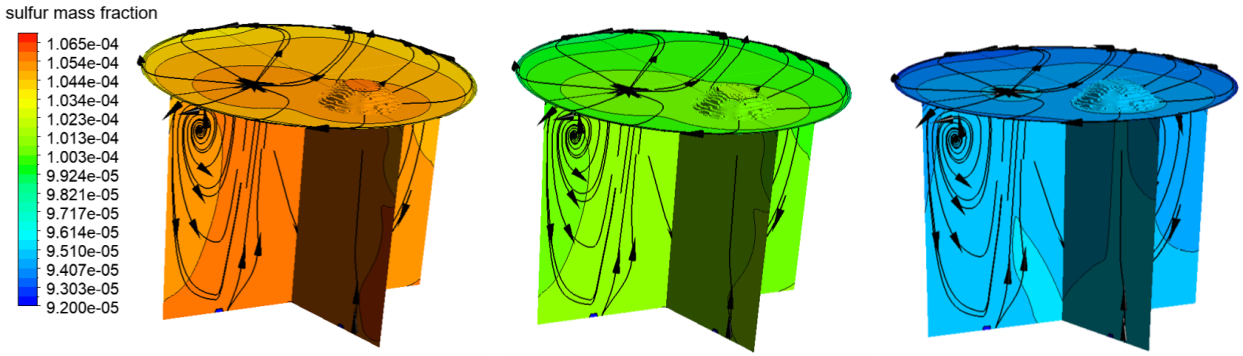

(a) (b) (c)

Figure 3.19. Sulfur content distribution at different time in the 90°-5/20 SCFM scenario : (a) 100 s; (b) 300 s; (c) 600 s.

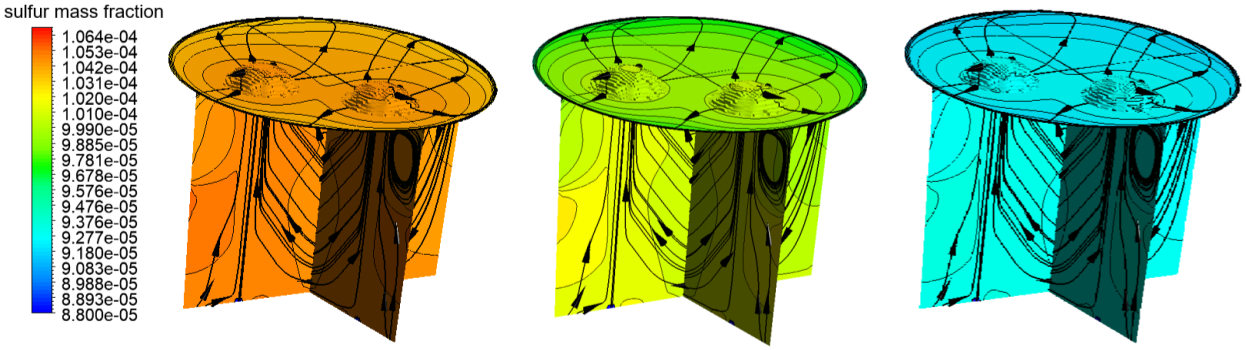

(a) (b) (c)

Figure 3.20. Sulfur content distribution at different time in the 90°-20/20 SCFM scenario : (a) 100 s; (b) 300 s; (c) 600 s.

temperatures, 1803 K, 1833 K, and 1863 K, are used in the 90°-5/5 SCFM ladle. It is still assumed that the temperature does not vary with time in each scenario, and the ladle is considered iso-thermal.

Table 3.3 summarizes the average oxygen activity a_O and sulfur distribution ratio L_S at the slag-steel interface in 300 seconds after the initiation of steel refining treatment in various scenarios. It is clear that the oxygen activity goes up as the temperature rises, and therefore the sulfur distribution ratio drops, resulting in the reduction of the term $[\% - S] - \frac{(\% - S)}{L_S}$ and desulfurization rate.

Table 3.3. Average a_O and L_S at the interface under different steel temperatures in 300 seconds

Temperature	a_O	L_S
1803 K	1.47×10^{-4}	951.30
1833 K	1.52×10^{-4}	940.86
1863 K	2.09×10^{-4}	829.16

Figure 3.21 depicts the transient sulfur removal rates for each of the three scenarios. It can be seen that the desulfurization rate slightly decreases when the steel temperature increases. This phenomenon supports the prior finding that the lower the oxygen activity, the bigger the sulfur distribution ratio, and the faster the desulfurization rate, as analyzed from Table 3.3. When the temperature rises from 1803 K to 1833 K and 1863 K, the overall desulfurization rate drops by 0.0159 % and 0.124 %, respectively. The impact of temperature on the desulfurization rate is relatively minimal compared to the enhancement rate of desulfurization by plug configuration and argon flow rate discussed previously. As a result, despite the fact that temperature adjustment can improve the desulfurization rate, it is probably not feasible in industrial treatment due to the weak effect.

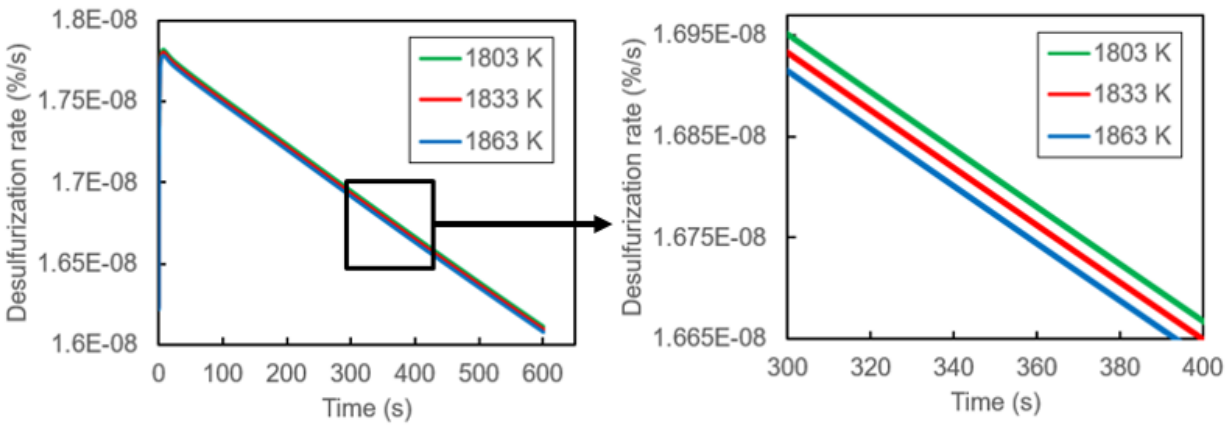

Figure 3.21. Sulfur mass fraction under different temperatures.

3.3.4 Effect of Initial (%-Al_2O_3) on Desulfurization Rate

As claimed previously, the [Al]-[O]-(Al_2O_3) equilibrium controls the oxygen activity at the slag-steel interface in this research. Different initial (%-Al_2O_3) values might lead to different oxygen activity and hence different desulfurization rates. Besides the 21.32 % initial Al_2O_3 mass fraction used in the baseline, two alternative beginning (%-Al_2O_3) values, 11.32 % and 29.32 %, are also utilized to simulate the desulfurization process in the 90°-5/5 SCFM ladle in this section to see how the initial (%-Al_2O_3) affect the reaction rate. The initial mass fractions of other oxides involved in the desulfurization process, including (%-SiO_2), (%-CaO), (%-MnO), (%-CaS), (%-FeO) and (%-MgO), are assumed to be constant, as is the sum of the initial (%-Al_2O_3) and the mass fraction of those species that do not participate in the reaction.

As listed in Table 3.4, the oxygen activity at the interface after 300 seconds of refining treatment marginally falls as the initial (%-Al_2O_3) grows. However, the sulfur distribution ratio L_S also significantly drops with the decrease of a_O. To explain this phenomenon, the slag sulfide capacity C_S in different scenarios are also summarized in Table 3.4. It indicates that the C_S decreases as the starting (%-Al_2O_3) grows, and thereby the L_S falls according to Equation 2.38, hindering the sulfur transport process from steel to slag. The transient sulfur removal rates for each of the three scenarios are visualized in Figure 3.22. It does reveal that the desulfurization rate is lower with a higher initial (%-Al_2O_3). Consequently, the initial (%-Al_2O_3) affects the desulfurization rate primarily by modifying C_S rather than a_O when utilizing the [Al]-[O]-(Al_2O_3) equilibrium approach to predict the sulfur removal rate. The desulfurization rate drops by 0.32 % and 1.55 % as the initial (%-Al_2O_3) increases from 11.32 % to 21.32 % and 29.32 %, respectively. Accordingly, the desulfurization process can be promoted by adequately adjusting the initial (%-Al_2O_3).

Table 3.4. Average a_O, L_S and C_S at the interface under different initial (%-Al_2O_3) in 300 seconds

Initial (%-Al_2O_3)	a_O	L_S	C_S
11.32 %	1.5187×10^{-4}	1396.01	2.67×10^{-2}
21.32 %	1.5186×10^{-4}	940.86	1.80×10^{-2}
29.32 %	1.5185×10^{-4}	406.60	7.78×10^{-3}

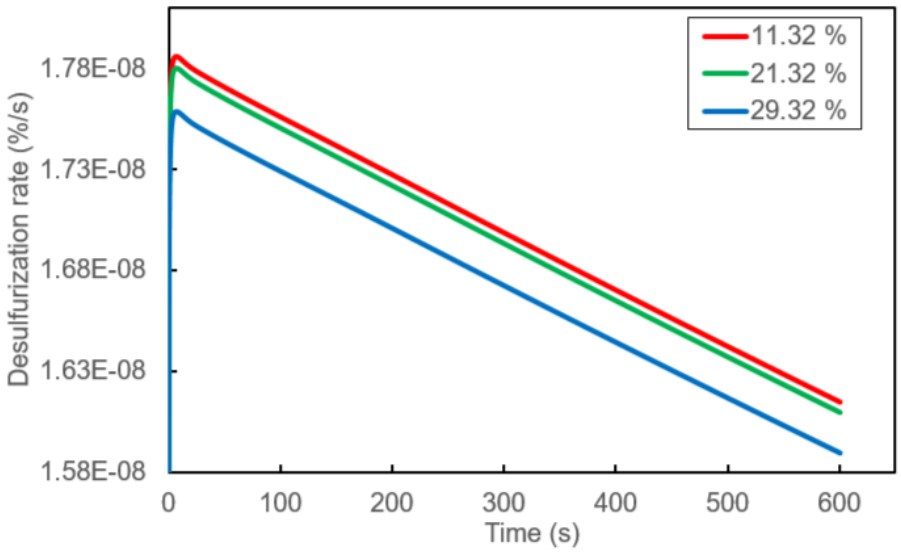

Figure 3.22. Sulfur mass fraction under different initial (%-Al_2O_3).

4. CONCLUSION

The desulfurization processes during secondary steelmaking in a ladle metallurgical furnace have been investigated using a 3D multiphase computational fluid dynamics model. The impacts of different scenarios on the desulfurization rate are explored in a Nucor simplified ladle with two bottom injection plugs in order to select the most appropriate operating parameters. The simulating domain is updated in terms of the slag eye location, slag eye size, and interface shape when the multiphase flow field becomes a quasi-steady state in each scenario, and only the steel phase remains in the computational domain. The desulfurization rate is computed by both the species transport model in ANSYS Fluent software and the user-defined functions based on mathematical desulfurization models.The main conclusions are listed as follows:

1. The VOF-DPM multiphase model can predicate the slag eye's size and location and the shape of the interface, making it more reliable to reflect the actual case than the flat surface;

2. The [Al]-[O]-(Al_2O_3) equilibrium method can accurately predict the desulfurization process, and the simulation result is comparable to that of (Al_2O_3)-(FeO)-(SiO_2)-(MnO)-[O]-[S] equilibrium method, but with simpler computer procedures and less time spent;

3. The velocity and turbulence dissipation rate in the steel domain are highest in the argon-bubble plume area and gradually decrease from the plug to the interface. In the bumps at the interface, the steel velocity is low while the turbulence dissipation rate is significant, leading to a high mass transfer coefficient k_m at the interface;

4. The 90°-20/20 SCFM scenario has the highest desulfurization rate, followed by the 90°-5/20 SCFM scenario and the 180°-5/5 SCFM scenario. The lowest desulfurization rate is found in the 90°-5/5 SCFM scenario. The 180° separation angle facilitates desulfurization better than the 90° separation angle at the same argon flow rate;

5. The distribution pattern of sulfur molar flux at the interface is analogous to the k_m distribution, indicating that the species transfer process influences the desulfurization rate. The oxygen activity at the interface increases over time, lowering the sulfur distribution ratio and slowing the desulfurization rate;

6. The sulfur content is high in the argon-bubble plume, and it continues to decrease from the plug to the interface. The desulfurization rate is high in the bump at the interface, but the sulfur content is also high, indicating that the sulfur removal rate is slower than the sulfur supplement rate. The mass transfer coefficient k_m and the difference in sulfur mass fraction between the current and equilibrium states act as limiting factors;

7. The effects of temperature on sulfur removal can be overlooked due to the minor variations in the desulfurization rate. Temperature influences the desulfurization rate by adjusting the a_O, whereas the initial (%-Al_2O_3) influences the rate mainly through changing C_S. Steel desulfurization is aided by a lower starting (%-Al_2O_3).

REFERENCES

[1] K. EL, E. KADDAH, *et al.*, "Mathematical model for desulphurization kinetics in argon-stirred ladles," 1981.

[2] S. BAN-YA, M. HINO, and H. TAKEZOE, "Thermodynamic properties of feto-na2o, feto-sio2-na2o, feto-p2o5-na2o and feto-p2o5-sio2-na2o slags," *Transactions of the Iron and Steel Institute of Japan*, vol. 25, no. 11, pp. 1122–1131, 1985.

[3] S. Ban-Ya, "Mathematical expression of slag-metal reactions in steelmaking process by quadratic formalism based on the regular solution model," *ISIJ international*, vol. 33, no. 1, pp. 2–11, 1993.

[4] C. Fincham and F. D. Richardson, "The behaviour of sulphur in silicate and aluminate melts," *Proceedings of the Royal Society of London. Series A. Mathematical and Physical Sciences*, vol. 223, no. 1152, pp. 40–62, 1954.

[5] I. Sommerville *et al.*, "The composition and temperature dependence of the sulfide capacity of metallurgical slags," *Metallurgical Transactions B*, vol. 17, no. 2, pp. 331–337, 1986.

[6] R. Young, J. Duffy, G. Hassall, and Z. Xu, "Use of optical basicity concept for determining phosphorus and sulphur slag-metal partitions," *Ironmaking & steelmaking*, vol. 19, no. 3, pp. 201–219, 1992.

[7] M. A. Andersson, P. G. Jönsson, and M. M. Nzotta, "Application of the sulphide capacity concept on high-basicity ladle slags used in bearing-steel production," *ISIJ international*, vol. 39, no. 11, pp. 1140–1149, 1999.

[8] L. Jonsson, D. Sichen, and P. Jönsson, "A new approach to model sulphur refining in a gas-stirred ladle–a coupled cfd and thermodynamic model," *ISIJ international*, vol. 38, no. 3, pp. 260–267, 1998.

[9] M. A. Andersson, L. T. Jonsson, and P. G. Jönsson, "A thermodynamic and kinetic model of reoxidation and desulphurisation in the ladle furnace," *ISIJ international*, vol. 40, no. 11, pp. 1080–1088, 2000.

[10] M. A. Andersson, P. G. Jönsson, and M. Hallberg, "Optimisation of ladle slag composition by application of sulphide capacity model," *Ironmaking & steelmaking*, vol. 27, no. 4, pp. 286–293, 2000.

[11] P. G. Jönsson and L. T. Jonsson, "The use of fundamental process models in studying ladle refining operations," *ISIJ international*, vol. 41, no. 11, pp. 1289–1302, 2001.

[12] M. Andersson, M. Hallberg, L. Jonsson, and P. Jönsson, "Slag-metal reactions during ladle treatment with focus on desulphurisation," *Ironmaking & steelmaking*, vol. 29, no. 3, pp. 224–232, 2002.

[13] A. Conejo, F. Lara, M. Macias-Hernández, and R. Morales, "Kinetic model of steel refining in a ladle furnace," *steel research international*, vol. 78, no. 2, pp. 141–150, 2007.

[14] W. Lou and M. Zhu, "Numerical simulation of desulfurization behavior in gas-stirred systems based on computation fluid dynamics–simultaneous reaction model (cfd–srm) coupled model," *Metallurgical and Materials Transactions B*, vol. 45, no. 5, pp. 1706–1722, 2014.

[15] Q. Cao, L. Nastac, A. Pitts-Baggett, and Q. Yu, "Numerical investigation of desulfurization kinetics in gas-stirred ladles by a quick modeling analysis approach," *Metallurgical and Materials Transactions B*, vol. 49, no. 3, pp. 988–1002, 2018.

[16] Q. Cao and L. Nastac, "Mathematical modelling of slag–metal reactions and desulphurization behaviour in gas-stirred ladle based on the dpm-vof coupled model," *Ironmaking & Steelmaking*, 2019.

[17] T. Z. Harmathy, "Velocity of large drops and bubbles in media of infinite or restricted extent," *AIChE Journal*, vol. 6, no. 2, pp. 281–288, 1960.

[18] J. Aoki, B. G. Thomas, J. Peter, and K. D. Peaslee, "Experimental and theoretical investigation of mixing in a bottom gas-stirred ladle," 2004.

[19] H. Laux and S. T. Johansen, "A cfd analysis of the air entrainment rate due to a plunging steel jet combining mathematical models for dispersed and separated multiphase flows," *Fluid Flow Phenomena in Metals Processing*, pp. 21–30, 1999.

[20] Q. Pan, "Modelling of turbulent flows with strong dispersed phase-continuous fluid interactions," 2014.

[21] D. Roy, P. C. Pistorius, and R. J. Fruehan, "Effect of silicon on the desulfurization of al-killed steels: Part i. mathematical model," *Metallurgical and Materials Transactions B*, vol. 44, no. 5, pp. 1086–1094, 2013.

[22] D. Ghosh, V. Krishnamurthy, and S. Sankaranarayanan, "Application of optical basicity to viscosity of high alumina blast furnace slags," *Journal of Mining and Metallurgy, Section B: Metallurgy*, vol. 46, no. 1, pp. 41–49, 2010.

[23] T. Mori, "On the phosphorus distribution between slag and steel," *Bull. Jap. Inst. Metals*, vol. 23, no. 4, pp. 354–361, 1984.

[24] Y. M. Krishna, T. Sowmya, and S. R. Sankaranarayanan, "Application of optical basicity parameter to foaming of slags," *la metallurgia italiana*, 2008.

[25] T. Engh, *Principles of metal refining*, 1992.

[26] Q. Cao, "Mathematical modeling of the fluid flow, multicomponent slag-metal reactions and desulfurization efficiency in gas-stirred ladles," Ph.D. dissertation, The University of Alabama, 2018.

[27] Q. Wang, Z. He, G. Li, B. Li, C. Zhu, and P. Chen, "Numerical investigation of desulfurization behavior in electroslag remelting process," *International Journal of Heat and Mass Transfer*, vol. 104, pp. 943–951, 2017.

[28] A. Harada, N. Maruoka, H. Shibata, and S.-y. Kitamura, "A kinetic model to predict the compositions of metal, slag and inclusions during ladle refining: Part 1. basic concept and application," *ISIJ international*, vol. 53, no. 12, pp. 2110–2117, 2013.

[29] J. C. Lamont and D. Scott, "An eddy cell model of mass transfer into the surface of a turbulent liquid," *AIChE Journal*, vol. 16, no. 4, pp. 513–519, 1970.

[30] U. Manual, "Ansys fluent 12.0," *Theory Guide*, 2009.